

# ***THM Coupled Process Modeling with TOUGH- FLAC to Evaluate the Fate and Transport of Water in a Salt-Based Repository***

**Fuel Cycle Research & Development**

*Prepared for  
U.S. Department of Energy  
Used Fuel Disposition*

*Jonny Rutqvist*

*Laura Blanco-Martin*

*Jim Houseworth*

*Lawrence Berkeley National Laboratory*

*September, 2012*

FCRD-UFD-2012-000297



**DISCLAIMER**

This information was prepared as an account of work sponsored by an agency of the U.S. Government. Neither the U.S. Government nor any agency thereof, nor any of their employees, makes any warranty, expressed or implied, or assumes any legal liability or responsibility for the accuracy, completeness, or usefulness, of any information, apparatus, product, or process disclosed, or represents that its use would not infringe privately owned rights. References herein to any specific commercial product, process, or service by trade name, trade mark, manufacturer, or otherwise, does not necessarily constitute or imply its endorsement, recommendation, or favoring by the U.S. Government or any agency thereof. The views and opinions of authors expressed herein do not necessarily state or reflect those of the U.S. Government or any agency thereof.

**FCT Quality Assurance Program Document**

Revision 1 08/19/2011

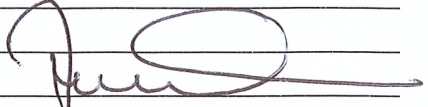
## Appendix E FCT Document Cover Sheet

Name/Title of Deliverable/Milestone Status of UFD Campaign International Activities in Disposal Research

Work Package Title and Number CX International – LBNL

Work Package WBS Number FT-12LB081102

Responsible Work Package Manager 1.02.08.11

Jens Birkholzer   
(Name/Signature)

Date Submitted 8/14/2012

Quality Rigor Level for Deliverable/Milestone  QRL-3  QRL-2  QRL-1  N/A\*  
 Nuclear Data

This deliverable was prepared in accordance with Lawrence Berkeley National Laboratory  
(Participant/National Laboratory Name)

QA program which meets the requirements of  
 DOE Order 414.1  NQA-1-2000  Other

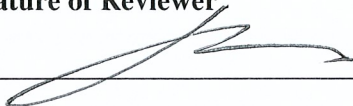
**This Deliverable was subjected to:**

Technical Review  Peer Review

**Technical Review (TR)**

**Review Documentation Provided**  
 Signed TR Report or,  
 Signed TR Concurrence Sheet or,  
 Signature of TR Reviewer(s) below

**Name and Signature of Reviewer**

Hui-Hai Liu   
\_\_\_\_\_  
\_\_\_\_\_

**Peer Review (PR)**

**Review Documentation Provided**  
 Signed PR Report or,  
 Signed PR Concurrence Sheet or,  
 Signature of PR Reviewer(s) below

**\*NOTE** In some cases there may be a milestone where an item is being fabricated, maintenance is being performed on a facility, or a document is being issued through a formal document control process where it specifically calls out a formal review of the document. In these cases, documentation (e.g., inspection report, maintenance request, work planning package documentation or the documented review of the issued document through the document control process) of the completion of the activity along with the Document Cover Sheet is sufficient to demonstrate achieving the milestone. QRL for such milestones may be also be marked N/A in the work package provided the work package clearly specifies the requirement to use the Document Cover Sheet and provide supporting documentation.

This page is intentionally blank.

## **CONTENTS**

1.	Introduction .....	1
2.	Coupled Processes and Water Flow Associated with Radioactive Waste Disposal in Salt.....	2
3.	TOUGH-FLAC and Salt Coupled Processes Modeling .....	4
4.	Creep Models Implemented in FLAC3D .....	7
4.1	The Maxwell model .....	7
4.2	The Burgers model.....	8
4.3	The Norton model .....	9
4.4	The WIPP model.....	10
4.5	The crushed salt model .....	11
5.	The Lux/Wolters constitutive model .....	11
6.	Modeling of an Overpressured Fluid-Injection and Salt-Damage Experiment .....	14
6.1	Experimental Set-up and Results .....	14
6.2	TOUGH2-EOS9 Model and Results.....	17
6.3	TOUGH-FLAC EOS4 Model and Results.....	21
7.	FLAC3D Simulation Using the Lux/Wolters Model and the Large-Strain Mode .....	26
8.	Generic Salt-Based Repository Model for THM Analysis.....	30
9.	Conclusions .....	34
10.	Acknowledgements .....	35
11.	References .....	36

## FIGURES

<b>Figure 1.</b> Microstructural observations on samples subjected to various injection pressures (Popp and Minkley, 2010).....	3
<b>Figure 2.</b> Experimental results on the evolution of permeability and gas accessible porosity versus strain (Popp et al., 2001).....	3
<b>Figure 3.</b> Schematic of linking TOUGH2 with FLAC <sup>3D</sup> for a coupled THM simulation. ....	5
<b>Figure 4.</b> The Maxwell model.....	8
<b>Figure 5.</b> The Burgers model. ....	8
<b>Figure 6.</b> Domain diagram for fluid injection into rock salt. ....	15
<b>Figure 7.</b> Experimental salt infiltration data from Clausthal University showing fluid pressure, stress, temperature, and infiltration volume over 6 days (axialdruck = axial stress, fluiddruck = fluid pressure, infiltriertes fluidvolumen = infiltrated fluid volume, manteldruck = confining stress, raumtemperatur = room temperature, and T-kompensiert= temperature compensated). ....	16
<b>Figure 8.</b> Rock salt sample sliced in half showing injection fluid tracer to fluoresce under an ultraviolet light. ....	17
<b>Figure 9.</b> Log permeability as a function of $\Delta pf$ . ....	18
<b>Figure 10.</b> Saturation profiles at 6 days (a) Saturation computed using modified TOUGH2-EOS9; (b) fluorescent green dye pattern from rock salt fluid-injection experiment. ....	20
<b>Figure 11.</b> Cumulative injected fluid as a function of time.....	21
<b>Figure 12.</b> Injected fluid volume as a function of time with comparison of TOUGH-FLAC full stress analysis with that of TOUGH-FLAC simplified stress analysis.....	23
<b>Figure 13.</b> Evolution of fluid liquid saturation in the case of TOUGH-FLAC simple stress analysis.....	24
<b>Figure 14.</b> Evolution of fluid liquid saturation in the case of TOUGH-FLAC full stress analysis.....	25
<b>Figure 15.</b> Distribution of (a) least compressive principal stress and (b) least compressive effective stress at 6 days. ....	26
<b>Figure 16.</b> Geometry of the model and zones defined for a rock-salt cavern. ....	26
<b>Figure 17.</b> Von Mises equivalent stress distribution obtained after 100 years.....	28
<b>Figure 18.</b> Contour of displacement (in meters) around the cavern after 100 years. ....	28
<b>Figure 19.</b> Evolution of cavern convergence over time. ....	29
<b>Figure 20.</b> Contour of displacement (in meters) around the cavern after 100,000 years. ....	30
<b>Figure 21.</b> (a) Typical layout of a high-level waste repository in salt including emplacement in horizontal tunnels, and (b) cross-section from the TSDE <i>in situ</i> heater experiment at Asse mine (Bechthold et al., 2004). ....	31
<b>Figure 22.</b> 2-D model grid for modeling of a horizontal nuclear waste emplacement tunnel in salt with the dimension of the waste package and tunnel given in Figure 21. ....	32
<b>Figure 23.</b> TOUGH2 simulation results of the evolution of (a) temperature, (b) liquid saturation and (c) pore pressure.....	33

## **ACRONYMS**

GDSE	Generic Disposal System Environment
IFD	integral finite differences
LBNL	Lawrence Berkeley National Laboratory
PWR	Pressurized Water Reactor
THM	thermal-hydrological-mechanical
TSDE	thermal simulation of drift emplacement
UFD	Used Fuel Disposition
WIPP	Waste Isolation Pilot Plant

This page is intentionally blank.



## 1. Introduction

In this report, we present FY2012 model development and initial simulations related to coupled thermal-hydrological-mechanical (THM) process modeling to evaluate the fate and transport of water in a salt-based repository. This work leverages existing computational models and tools to couple THM phenomena in salt under subsurface repository conditions, with the added focus on brine accessibility and moisture transport. In FY2012, LBNL's work aimed at exploring and demonstrating the capabilities of the current modeling tool (TOUGH-FLAC) for simulating temperature-driven coupled flow and geomechanical processes in salt. This includes development related to, and implementation of, necessary capabilities and testing the model against relevant information and published experimental data related to the fate and transport of water.

TOUGH-FLAC (Rutqvist et al., 2002; Rutqvist, 2011) is a numerical simulator based on LBNL's TOUGH2 multiphase flow simulator (Pruess et al., 2011) and the FLAC<sup>3D</sup> geomechanical simulator (Itasca, 2009). Over the last 10 years, TOUGH-FLAC has been applied to a wide range of geoscientific research and geoengineering applications, including CO<sub>2</sub> sequestration, geothermal energy extraction, gas production from hydrate-bearing sediments, underground compressed-air-energy storage, and nuclear waste disposal in open or bentonite-backfilled tunnels in fractured tuff, granite, or clay host rock (Rutqvist, 2011). The wealth of available fluid-equations-of-state modules in TOUGH2 and geomechanical constitutive models in FLAC<sup>3D</sup>, as well as the possibility for code modifications, provides the required flexibility for extending and applying the TOUGH-FLAC simulator to a wide range of specialized applications, including salt coupled processes. The TOUGH2 and FLAC<sup>3D</sup> combination has until recently not been applied for modeling coupled processes in salt. However, the FLAC<sup>3D</sup> code has been widely used for modeling of salt geomechanics (i.e., without taking into account water flow and transport), especially in Germany (Wolters et al., 2012; Hampel et al., 2010) but also in the United States (associated with the Waste Isolation Pilot Plant [WIPP] site), and includes a number of constitutive geomechanics models capable of modeling visco-plastic creep for both solidified and crushed salt (Itasca, 2009).

The work presented here is based on cooperation between LBNL and a research group led by Professor Lux at Clausthal University in Germany, a world-leading research institution for salt geomechanics. The collaboration involves the use of coupled FLAC<sup>3D</sup> and TOUGH2 simulations to simulate salt coupled-THM processes. One part of this collaboration the implementation of more advanced constitutive models for application to tunnel-scale problems. In this work, we expand on our collaboration to advance the development for application of TOUGH-FLAC to the United States salt repository program, with special focus on high-temperature coupled processes and their effect on brine migration. This includes implementation and testing of the Lux/Wolters salt constitutive geomechanics model (Wolters et al., 2012) within TOUGH-FLAC. The Lux/Wolters model has been established on the basis of numerous laboratory investigations designed to study, from a macroscopic viewpoint, the mechanisms involved in the damage and healing of rock salt. This includes formation of secondary permeability caused by damage at high shear stress, as well as fluid infiltration along grain interfaces at low effective stress. Another key component required for modeling of salt caverns is the ability to simulate large

deformations associated with creep, closure, and sealing of underground tunnels and caverns over the longer term (i.e., 10,000 years).

In this report, we first describe the TOUGH-FLAC simulator, the various constitutive models for creep and salt geomechanics that are available in FLAC<sup>3D</sup>, and the Lux/Wolters constitutive model. We then present a number of model simulations using TOUGH-FLAC and the Lux/Wolters constitutive model, including modeling of a laboratory experiment related to fluid infiltration into a bench-scale salt sample, modeling of a salt cavern undergoing convergence caused by creep and large deformation, and high-temperature multiphase flow processes around a waste emplacement tunnel. These simulations include processes and features that will be required for coupled THM modeling of a salt repository with respect to the fate and transport of water. We conclude that the TOUGH-FLAC combination can provide the necessary modeling tool for simulating coupled processes associated with disposal of high-level nuclear waste in salt formations, including modeling of high-temperature, multiphase flow and transport processes, coupled with time-dependent geomechanical (creep) processes with large deformations.

## 2. Coupled Processes and Water Flow Associated with Radioactive Waste Disposal in Salt

For modeling of salt coupled processes and water flow, we have to define the general requirements of such a model based on the current state of knowledge. It is clear that disposal in salt formations differs in an essential way from other host rock options, e.g., clay and crystalline. Rock salt in the undisturbed state typically has an extremely low permeability ( $\sim 10^{-21}$  m<sup>2</sup>) and low water content (<1%), which are significant positive attributes for disposal of radioactive waste. For undisturbed rock salt, numerous examples demonstrate the ability of such a rock mass to behave as a nearly impermeable barrier to fluid flow over geologic time periods. A significant challenge for radioactive waste disposal in salt is to preserve these positive attributes under repository conditions where effects such as drift-wall convergence, thermo-mechanically induced stress redistribution, and local damage can alter rock properties (Minkley and Popp, 2010).

Although salt has very low permeability in undisturbed conditions, many laboratory experiments and field tests have shown that given sufficient deviatoric stress, or alternatively, sufficient pore pressure, salt rock will enter a dilatant regime in which microfractures develop along grain boundaries, as shown in Figure 1 (Popp et al., 2001; Minkley and Popp 2010). Such stress conditions are present in the disturbed rock zone around excavations in salt. The microfracturing leads to large increases in permeability compared to the undisturbed condition. As shown in laboratory experiments, the permeability can increase by several orders of magnitude after a few percent of axial strain under increasing deviatoric (shear) stress, as shown in Figure 2 (Popp et al., 2001). Thus, one of the key requirements for our model will be to properly simulate the stress- and fluid-pressure-induced permeability evolution over time, meaning that we need an appropriate constitutive model and model parameters for applying such a model to study the fate and transport of water. Consequently, our first step in model development is to implement such a constitutive model, and then test the implementation and model by simulating laboratory

experiments, such as laboratory experiments on salt dilatancy and permeability enhancement caused by fluid overpressure, and associated fluid migration.

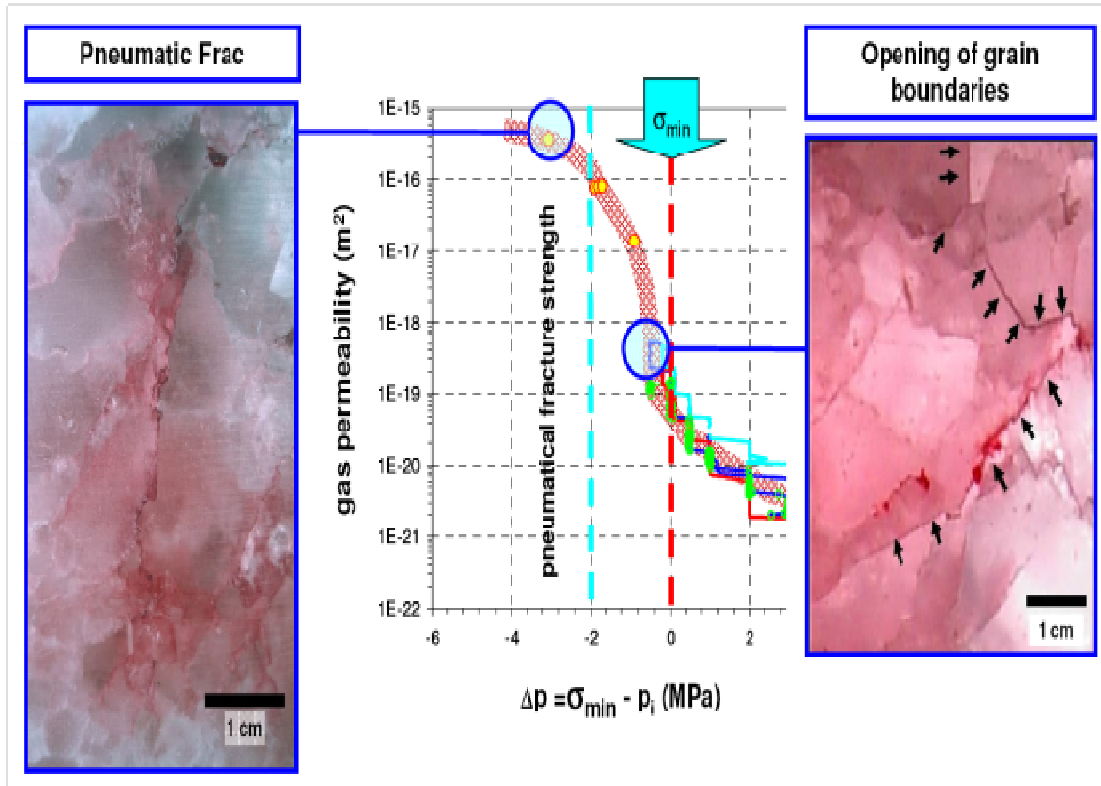


**Figure 1.** Microstructural observations on samples subjected to various injection pressures (Popp and Minkley, 2010).

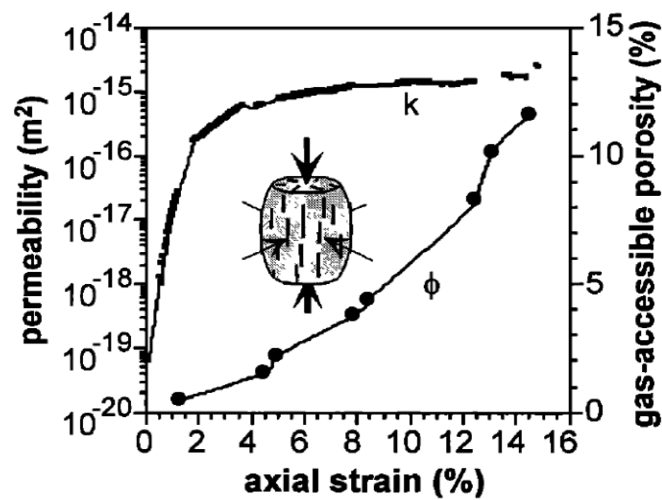


**Figure 2.** Experimental results on the evolution of permeability and gas accessible porosity versus strain (Popp et al., 2001).

### 3. TOUGH-FLAC and Salt Coupled Processes Modeling

In this section, we describe the current TOUGH-FLAC simulator and the required additional developments for modeling salt coupled processes. We first briefly describe the two codes TOUGH2 and FLAC<sup>3D</sup>, then the current TOUGH-FLAC simulator, and finally discuss how it can be extended for applications to modeling salt coupled processes.

TOUGH2 is LBNL's in-house model developed for multidimensional fluid and heat flows of multiphase, multicomponent fluid mixtures in porous and fractured media (Pruess et al., 2011). The first version was developed in the early 1980s, primarily for geothermal reservoir engineering, but now is widely used at universities, government organizations, and private industry for applications to nuclear waste disposal, environmental remediation problems, energy production from geothermal, oil, and gas reservoirs, as well as gas hydrate deposits, geological carbon sequestration, and vadose zone hydrology. TOUGH2 uses space discretization by integral finite differences (IFD), for 1-D, 2-D, 3-D regular or irregular grid geometries, and is applicable to single porosity or multi-continua (fractured media). It uses fully implicit time weighting with simultaneous, iterative solution of all mass and energy balances, and phase (dis-)appearance is handled by switching primary variables. Currently, a suite of TOUGH simulators is continually updated, with new equation-of-state (EOS) modules being developed, and refined process descriptions implemented into the TOUGH framework. For example, in the case of high temperature nuclear waste disposal, involving temperatures up to 200°C, the EOS4 equation of state module has been extensively applied and validated against field experiments, especially in welded fractured tuff.

FLAC<sup>3D</sup> is one of several numerical simulators developed by the ITASCA geomechanics consulting company for rock and soil mechanics applications (Itasca, 2009). FLAC<sup>3D</sup> simulates the behavior of three-dimensional structures built of soil, rock, or other materials that undergo plastic flow when their yield limits are reached. Materials are represented by polyhedral elements within a three-dimensional grid that is adjusted by the user to fit the shape of the object to be modeled. Each element behaves according to a prescribed linear or nonlinear stress/strain law in response to applied forces or boundary restraints. The material can yield and flow, and the grid can deform (in large-strain mode) and move along with the material represented. The explicit, Lagrangian calculation scheme and the mixed-discretization zoning technique used in FLAC<sup>3D</sup> ensure that plastic collapse and flow are modeled very accurately. Because no matrices are formed, large three-dimensional calculations can be made without excessive memory requirements. The drawbacks of explicit formulation (i.e., small time-step limitations and the question of required damping) are overcome by automatic inertia scaling and automatic damping that does not influence the mode of failure. In such an explicit scheme, a large-strain simulation is hardly more time-consuming than a small-strain run, because there is no stiffness matrix to be updated. The program has 13 basic built-in material models: the "null" model; three elasticity models (isotropic, transversely isotropic, and orthotropic elasticity); and nine plasticity models (Drucker-Prager, Mohr-Coulomb, strain-hardening/softening, ubiquitous-joint, bilinear strain-hardening/softening ubiquitous-joint, double-yield, modified Camclay, Cysoil and Hoek-Brown). Related to salt geomechanics, there are eight optional material models available that simulate time-dependent (creep) material behavior: (1) the classical viscoelastic (Maxwell) model; (2) a Burgers substance viscoelastic model; (3) a two-component power law; (4) a reference creep

formulation (the WIPP model) implemented for nuclear waste isolation studies; (5) a Burgers-creep viscoplastic model combining the Burgers model and the Mohr-Coulomb model; (6) a power-law viscoplastic model combining the two-component power law and the Mohr-Coulomb model; (7) a WIPP-creep viscoplastic model combining the reference creep formulation with the Drucker-Prager plasticity model; and (8) a “crushed-salt” model that simulates both volumetric and deviatoric creep compaction.

For analysis of coupled THM problems, the TOUGH2 and FLAC<sup>3D</sup> are executed on compatible numerical grids and linked through a coupled THM model (Figure 3) with coupling functions serving to pass relevant information between the field equations that are solved in respective code. Depending on the problem and specific porous media (e.g., fractured rock, unsaturated clay, hydrate-bearing sediments), a number of coupling functions have been developed.

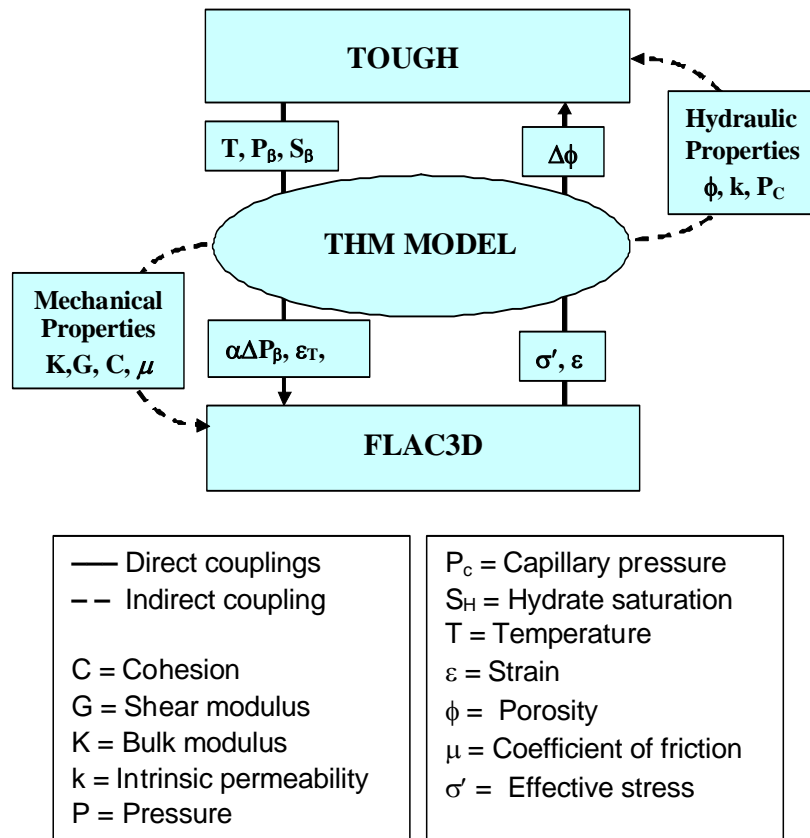


Figure 3. Schematic of linking TOUGH2 with FLAC<sup>3D</sup> for a coupled THM simulation.

In Figure 3, the data exchanges between TOUGH and FLAC<sup>3D</sup> are illustrated with arrows going through the central THM model. The arrow on the right-hand side of Figure 3 shows the transmission of the effective stress  $\sigma'$  and strain  $\epsilon$  (that are computed in FLAC<sup>3D</sup>) to TOUGH for calculation of the updated porosity  $\phi$  and the corresponding porosity change  $\Delta\phi$ . This

mechanically induced  $\Delta\phi$  has an immediate effect on fluid flow behavior. For example, if a change in  $\sigma'$  and  $\varepsilon$  causes  $\phi$  to decrease, the pore pressure is expected to rise, especially if the permeability is low. The computed  $\Delta\phi$  is then used to estimate changes in  $k$  by means of empirical equations. The updated  $\phi$  and  $k$  values are in turn used to estimate changes in the hydraulic and capillary properties of the porous medium (i.e., aqueous- and gas-phase relative permeabilities  $k_{rA}$  and  $k_{rG}$ , and capillary pressure  $P_c$ ) by employing appropriate scaling equations. For fractured media, a similar exponential empirical model has been applied to correct permeability for changes in the stress field (e.g., Rutqvist et al., 2002).

The arrow on the left side of Figure 3 depicts the flow of data obtained from TOUGH2 (namely the pressure  $P$ , temperature  $T$ , and phase saturations  $S_\beta$ ) to FLAC<sup>3D</sup> for processing and estimation of their impact on the effective stress through the term  $\alpha\Delta P_\beta$  ( $\alpha$  being Biot's effective stress parameter), as well as on thermal and swelling strains ( $\varepsilon_T$  and  $\varepsilon_{sw}$ , respectively).

Additionally, changes in  $P$ ,  $T$ , and  $S_\beta$  may also result in changes in other mechanical properties listed in Figure 3. These include the bulk modulus  $K$ , the shear modulus  $G$ , the cohesion  $C$ , and the coefficient of internal friction  $\mu$ . For example, in the case of hydrate-bearing sediment, geomechanical properties change as a function of solid-phase saturations, i.e., hydrate and ice saturations ( $S_H$  and  $S_I$ , respectively). In the case of unsaturated soil, the bulk modulus and friction angle is a function of suction.

As described in Rutqvist (2011), three possible coupling schemes—Jacobian, iterative, and time-step—may be used for linking TOUGH2 and FLAC<sup>3D</sup>. The Jacobian is the highest level of iterative coupling, in which all the geomechanical and flow parameters are continuously updated (in every Newtonian iteration of every time step), and their changes are accounted for in the computation of the Jacobian matrix. However, most applications to date have been utilizing time-step coupling involving correction of the geomechanical and flow parameters once in (i.e., at the end of) each time step. It was expected that the full Jacobian scheme would be necessary for problems in which pore-volume (direct) couplings dominate, i.e., when a mechanically induced  $\Delta\phi$  gives rise to a relatively strong and rapid change in pore pressure, and where it is necessary to rigorously preserve the fluid mass and heat balances. For problems in which the so-called property-changes (indirect) couplings are predominant, iterative or time-step coupling schemes are sufficient.

It is well known that there could be serious stability issues for problems in which pore-volume coupling dominates, such as when a low-permeability porous medium is mechanically squeezed by an external force. However, as it turns out, the coupling of TOUGH and FLAC<sup>3D</sup> is equivalent to the coupling of a finite-volume reservoir simulator to a finite-element geomechanical simulator, which corresponds to a mixed formulation that is stable in space (Kim et al., 2012). Moreover, by choosing an appropriate coupling scheme with so-called stress fixed iterations in the sequential scheme, the solution becomes unconditionally stable. Recently, such a coupling scheme has been applied and tested for the linking of a TOUGH family module with FLAC<sup>3D</sup> (Kim et al., 2012).



For extension of TOUGH-FLAC to salt coupled processes, key components to be added involve (1) implementation of an advanced constitutive model for salt-creep behavior, including modeling of damage evolution and associated permeability changes, which are critical for modeling water migration, considering high-temperature effects; (2) development of an appropriate algorithm related to strong pore-volume coupling under large strain and deformation; and (3) development of appropriate coupling algorithms for time-dependent (creep) behavior. The first item (an advanced constitutive model for salt creep behavior) is solved by implementing the Lux/Wolters constitutive model, a model described in more detail in the next section. The second item (pore-volume coupling under large strain) will involve updating the numerical grid in TOUGH2 in response to the deforming mesh in FLAC<sup>3D</sup>, and to make sure that sudden pore-volume changes are correctly translated to pressure changes in TOUGH2. Finally, the third item (coupling under creep) will require an appropriate time-stepping scheme considering the fluid flow and creep time steps in TOUGH2 and FLAC<sup>3D</sup>. All these developments are modification to the existing code, but will require further verification and testing against experimental results.

## 4. Creep Models Implemented in FLAC3D

In this section we present the basic theory and equations related to available creep models that are part of the FLAC<sup>3D</sup> standard code with creep option invoked. In describing the creep models within the framework of creep behavior, both stress tensor and strain tensors are divided into deviatoric and volumetric parts, noting that creep processes are governed by the deviatoric part. The deviatoric stress and strain are respectively calculated using

$$s_{ij} = \sigma_{ij} - \frac{\sigma_{ll}}{3} \delta_{ij} \quad (1)$$

and

$$e_{ij} = \varepsilon_{ij} - \frac{\varepsilon_{ll}}{3} \delta_{ij} \quad (2)$$

In addition, several of the creep models described below use the Von Mises equivalent stress, which by definition reads

$$\sigma_v = \sqrt{3/2 s_{ij}s_{ij}} \quad (3)$$

### 4.1 The Maxwell model

The Maxwell model is the simplest creep model. In one dimension, it consists of a dashpot (that accounts for viscosity) in series with a spring (to represent the elastic response), as illustrated in Figure 4.

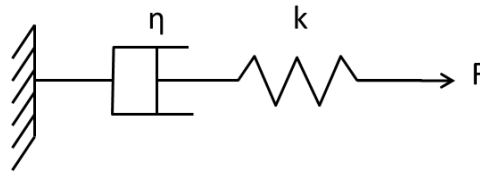


**Figure 4.** The Maxwell model.

The displacement rate reads

$$\dot{u} = \frac{\dot{F}}{k} + \frac{F}{\eta} \quad (4)$$

where  $k$  is the spring elastic constant and  $\eta$  is the viscosity. Note that the dot over a variable stands for a time derivative. To calculate the new displacement at the end of each time step  $\Delta t$ , the mean value of the force over  $\Delta t$  is retained (central difference).

In terms of stresses, the volumetric component is assumed to be purely elastic, so that the Maxwell response is included in the deviatoric part, which governs creep. The Maxwell model can be used both in creep and relaxation. In the former, the creep rate is constant; in the latter, the stress completely disappears. The material properties required for the Maxwell model are the elastic shear and bulk moduli,  $G$  and  $K$ , respectively, and the viscosity  $\eta$ .

## 4.2 The Burgers model

The Burgers model consists of a Maxwell model in series with a Kelvin model—see Figure 5.

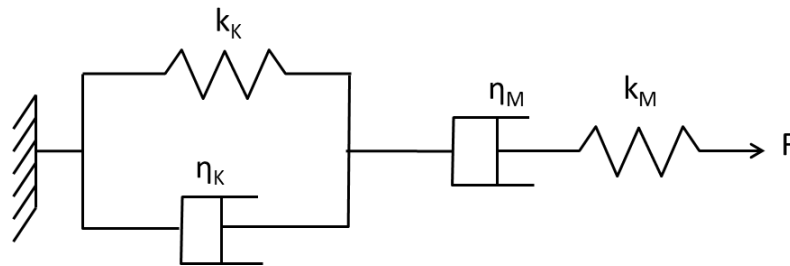


**Figure 5.** The Burgers model.

The total displacement rate reads:

$$\dot{u} = \dot{u}_K + \dot{u}_M = \frac{F - k_K u_K}{\eta_K} + \frac{\dot{F}}{k_M} + \frac{F}{\eta_M} \quad (5)$$

One particularity of the Kelvin model is that it does not account for instantaneous elasticity. Under a constant stress  $\sigma_0$ , the creep is limited to  $\sigma_0/E$ , and the creep rate is not constant. Furthermore, the Kelvin model is not suitable for relaxation, because under a constant strain  $\varepsilon_0$ ,



the stress does not disappear, but remains equal to  $E\varepsilon_0$ . As a result, the response of a Kelvin substance is dependent on past history.

In FLAC<sup>3D</sup>, the Kelvin and Maxwell displacement increments are combined to obtain the applied displacement increment. In terms of stress and strain, the material properties needed are:  $K$ ,  $G_K$ ,  $G_M$ ,  $\eta_K$ , and  $\eta_M$ .

In order to include visco-elasto-plastic responses, the Burgers model is associated with the Mohr-Coulomb criterion in the **Burgers-Creep Viscoplastic Model** implemented in FLAC<sup>3D</sup>. In this case, the volumetric response is elasto-plastic. The Mohr-Coulomb yield envelope accounts for shear and tensile yielding.

### 4.3 The Norton model

In the Norton power law, the creep strain-rate tensor is calculated using

$$\dot{\varepsilon}_{ij}^c = \frac{3 s_{ij}}{2 \sigma_v} \dot{\varepsilon}_{cr} \quad (6)$$

where

$$\dot{\varepsilon}_{cr} = A \sigma_v^n \quad (7)$$

Thus, the creep rate is proportional (co-axial) to the deviatoric stress. The volumetric component of the stress is assumed elastic:

$$\Delta \sigma_{ll} = 3K \dot{\varepsilon}_{ll} \Delta t \quad (8)$$

where  $\dot{\varepsilon}_{ij} = \dot{\varepsilon}_{ij}^e + \dot{\varepsilon}_{ij}^c$  is the total strain rate (note that  $\dot{\varepsilon}_{ll}^c = 0$ ). The deviatoric stress increments are given by

$$\Delta s_{ij} = 2G(\dot{\varepsilon}_{ij} - \dot{\varepsilon}_{ij}^c) \Delta t \quad (9)$$

In Equation 6, the averages of the new and old deviatoric stress components are used (except for the first iteration, in which the current values are taken).

The Norton model is often used to simulate the creep behavior of salt (Norton, 1929). To account for multiple creep mechanisms, FLAC<sup>3D</sup> includes a two-component law that reads

$$\dot{\varepsilon}_{cr} = \dot{\varepsilon}_1 + \dot{\varepsilon}_2 \quad (10)$$

where

$$\dot{\varepsilon}_1 = \begin{cases} A_1 \sigma_v^{n_1} & \sigma_v \geq \sigma_1^{ref} \\ 0 & \sigma_v < \sigma_1^{ref} \end{cases} \quad (11)$$

$$\dot{\varepsilon}_2 = \begin{cases} A_2 \sigma_v^{n_2} & \sigma_v \leq \sigma_2^{ref} \\ 0 & \sigma_v > \sigma_2^{ref} \end{cases} \quad (12)$$

Depending on the values of  $\sigma_1^{ref}$  and  $\sigma_2^{ref}$ , several options are possible. The material properties required by the Norton creep law are  $G$ ,  $K$ ,  $A_i$  and  $n_i$ . The visco-elastic Norton model is combined with the Mohr-Coulomb criterion in the **Power-Law Viscoplastic Model** implemented in FLAC<sup>3D</sup>. This way, shear and tensile yielding can be accounted for. In this case, the volumetric behavior is elasto-plastic.

#### 4.4 The WIPP model

The empirical WIPP (*Waste Isolation Pilot Plant*) model is also used to model the creep behavior of salt (Hermann et al., 1980). Its distinctive feature is that it accounts for the effect of temperature. As in the previous models, the volumetric stress is assumed to be purely elastic (Equation 8). For the deviatoric part, the creep strain rate is given by

$$\dot{\epsilon}_{ij}^c = \dot{\epsilon}_{ij}^c = \frac{3}{2} \frac{s_{ij}}{\sigma_v} \dot{\epsilon} \quad (13)$$

The scalar strain rate  $\dot{\epsilon}$  is composed of a primary and a secondary creep rate, which read respectively

$$\dot{\epsilon}_p = \begin{cases} (A - B\epsilon_p)\dot{\epsilon}_s & \dot{\epsilon}_s \geq \dot{\epsilon}_{ss} \\ [A - B(\dot{\epsilon}_{ss}/\dot{\epsilon}_s)\epsilon_p]\dot{\epsilon}_s & \dot{\epsilon}_s < \dot{\epsilon}_{ss} \end{cases} \quad (14)$$

and

$$\dot{\epsilon}_s = D\sigma_v^n \exp(-Q/RT) \quad (15)$$

where  $R$  is the universal gas constant,  $T$  is temperature and  $Q$  is the activation energy. The mean primary creep strain is calculated in the iterations using

$$\epsilon_p = \epsilon_p^{old} + \dot{\epsilon}_p \Delta t / 2 \quad (16)$$

The deviatoric stress increments are calculated using Equation (9). The material properties required by the WIPP model are  $K$ ,  $G$ ,  $A$ ,  $B$ ,  $\dot{\epsilon}_{ss}$ ,  $D$ ,  $n$ , and  $Q$ .

Finally, the WIPP model is combined with the Drucker-Prager criterion (shear and tensile yielding) in the **WIPP-Creep Viscoplastic Model** implemented in FLAC<sup>3D</sup>. Again, the volumetric response in this case is elasto-plastic. In addition, softening behavior is included using the second invariant of the deviatoric plastic strain increments:

$$\epsilon^{dp} = \epsilon^{dp} + \Delta t \sqrt{\dot{\epsilon}_{ij}^{dp} \dot{\epsilon}_{ij}^{dp} / 2} \quad (17)$$

## 4.5 The crushed salt model

This model is a variation of the WIPP model explained above and is useful for simulating volumetric and deviatoric creep compaction. Due to compaction, the density of the salt increases (as a function of the volumetric strain,  $\varepsilon_v$ ) from an initial value  $\rho_i$  to the intact salt density,  $\rho_f$ . The ratio between the current and the intact salt density,  $F_d = \rho/\rho_f$ , tracks the crushed-salt compaction. The rate of change of density is given by

$$\dot{\rho} = -\rho \dot{\varepsilon}_v \quad (18)$$

The crushed-salt model assumes that the creep compaction mechanism only takes place if the mean stress is compressive. Moreover, compaction is supposed irreversible (i.e., density cannot decrease) and bounded (i.e., no further compaction will occur after  $\rho_f$  has been reached). Apart from the elastic and viscous components, this model assumes that the strain-rate tensor has a third component that accounts for viscous compaction:

$$\dot{\varepsilon}_{ij}^c = \dot{\varepsilon}_v^c \left[ \frac{\delta_{ij}}{3} - \frac{\sigma_{ik}^d \delta_{kj}}{\sigma_v} \right] \quad (19)$$

where

$$\dot{\varepsilon}_v^c = \frac{1}{\rho} B_0 [1 - \exp(-B_1 \sigma)] \exp(B_2 \rho) \quad (20)$$

with  $\sigma = \sigma_{ii}/3$ . Thus  $\dot{\varepsilon}_{ii}^c \neq 0$ , and as a result, the volumetric response is not only elastic. As for the viscous shear strain rate, Equation 13 from the WIPP model is used. The primary creep strain rate is the same; however,  $\sigma_v$  is divided by the fractional density  $F_d$  in the secondary creep strain rate, so that

$$\dot{\varepsilon}_s = D \left( \frac{\sigma_v}{F_d} \right)^n \exp(-Q/RT) \quad (21)$$

The material properties required by the crushed-salt model are those described in the WIPP model plus  $B_0$ ,  $B_1$  and  $B_2$  (determined experimentally from isotropic compaction tests). Furthermore, the crushed-salt bulk and shear moduli depend on the density through a nonlinear empirical relationship (Itasca, 2009).

## 5. The Lux/Wolters constitutive model

The Lux/Wolters constitutive model has been developed at the Chair of Waste Disposal and Geomechanics, Clausthal University of Technology (Germany). It has been established on the basis of laboratory investigations designed to study, from a macroscopic viewpoint, the mechanisms involved in the damage and healing of rock salt (Wolters et al., 2012).

The Lux/Wolters model has been implemented and can be used in FLAC<sup>3D</sup>. With respect to the default models implemented in this software, the distinctive feature of the Lux/Wolters model is that the healing (or sealing) process is taken into account. Healing is important, because it reduces the dilatancy (i.e., volume variation) induced by damage (tensile or shear yielding).

In the Lux/Wolters model, the strain rate is composed of the superposition of four strain rates issued from different mechanisms: elastic, viscoplastic, damage-induced and healing processes. The strain rate tensor reads

$$\dot{\boldsymbol{\varepsilon}}_{ij} = \dot{\boldsymbol{\varepsilon}}_{ij}^e + \dot{\boldsymbol{\varepsilon}}_{ij}^{vp} + \dot{\boldsymbol{\varepsilon}}_{ij}^d + \dot{\boldsymbol{\varepsilon}}_{ij}^h \quad (22)$$

The elastic strain rate is divided into a deviatoric and a volumetric part, so that

$$\dot{\boldsymbol{\varepsilon}}_{ij}^e = \frac{1}{2 \cdot G} \cdot \frac{\dot{s}_{ij}}{1-D} + \frac{1}{9 \cdot K} \cdot \frac{\dot{\sigma}_{II}}{1-D} \cdot \delta_{ij} \quad (23)$$

The factor  $1-D$  accounts for the damage-induced reduction of the load-bearing cross-sectional area (*cf.* (Kachanov, 1986)), and is calculated from the damage rate  $\dot{D}$  defined below.

As in the previous models, the viscoplastic strain rate is purely deviatoric (i.e., there is no volumetric variation related to viscosity). The salt viscous response is inspired from the Burgers model; however, the parameters are now dependent on both the stress and the temperature. This corresponds to the Lubby2 constitutive model, also developed at Clausthal in the early 1980s (Lux, 1984). The introduction of the damage-induced reduction factor leads to

$$\dot{\boldsymbol{\varepsilon}}_{ij}^{vp} = \frac{3}{2} \cdot \left( \frac{1}{\bar{\eta}_k} \cdot \left( 1 - \frac{\varepsilon_{tr}}{\max \varepsilon_{tr}} \right) + \frac{1}{\bar{\eta}_m} \right) \cdot \frac{s_{ij}}{1-D} \quad (24)$$

where

$$\bar{\eta}_k = \bar{\eta}_k^* \cdot \exp\left(k_2 \cdot \frac{\sigma_v}{1-D}\right) \quad (25)$$

$$\max \varepsilon_{tr} = \frac{1}{\bar{G}_k} \cdot \frac{\sigma_v}{1-D} \quad (26)$$

$$\bar{G}_k = \begin{cases} \bar{G}_k^{**} \cdot \exp\left(k_1 \cdot \frac{\sigma_v}{1-D}\right) \cdot \exp(l_1 \cdot T) \cdot \left(\frac{\sigma_v}{\sigma^*}\right)^b & (\varepsilon_{tr} < \max \varepsilon_{tr}, \text{hardening}) \\ \bar{G}_{kE}^{**} \cdot \exp\left(k_{1E} \cdot \frac{\sigma_v}{1-D}\right) \cdot \exp(l_{1E} \cdot T) \cdot \left(\frac{\sigma_v}{\sigma^*}\right)^b & (\varepsilon_{tr} > \max \varepsilon_{tr}, \text{softening}) \end{cases} \quad (27)$$

$$\bar{\eta}_m = \bar{\eta}_m^{**} \cdot \exp\left(m \cdot \frac{\sigma_v}{1-D}\right) \cdot \exp(l \cdot T) \cdot \left(\frac{\sigma_v}{\sigma^*}\right)^a \quad (28)$$

Note that in Equations (27) and (28),  $\sigma^*=1$  MPa. The damage-induced strain rate has two components, one for tensile failure and one for shear failure, so that

$$\dot{\epsilon}_{ij}^d = \dot{\epsilon}_{ij}^{ds} + \dot{\epsilon}_{ij}^{dz} = a_3 \cdot \frac{\left\langle \frac{F^{ds}}{F^*} \right\rangle^{a_1}}{(1-D)^{a_2}} \cdot \frac{\partial Q^{ds}}{\partial \sigma_{ij}} + a_3 \cdot \frac{\left\langle \frac{F^{dz}}{F^*} \right\rangle^{a_1}}{(1-D)^{a_2}} \cdot \frac{\partial Q^{dz}}{\partial \sigma_{ij}} \quad (29)$$

where

$$\langle x \rangle = \begin{cases} 0 & x \leq 0 \\ x & x > 0 \end{cases} \quad (30)$$

In Equation (29),  $F^{ds}$  and  $F^{dz}$  are the shear and tensile yielding functions, respectively. Similarly,  $Q^{ds}$  and  $Q^{dz}$  stand for the shear and tensile plastic potential functions. Also,  $F^*=1$  MPa.

The last component of the strain-rate tensor corresponds to healing. Healing cannot occur while damage is taking place. Moreover, some damage is necessary before healing can actually start. The damage rate is defined as

$$\dot{D} = a_{15} \cdot \frac{\left( \left\langle \frac{F^{ds}}{F^*} \right\rangle + \left\langle \frac{F^{dz}}{F^*} \right\rangle \right)^{a_{16}}}{(1-D)^{a_{17}}} \quad (31)$$

This rate is positive if at least  $F^{ds} > 0$  or  $F^{dz} > 0$ . If both verify  $F^{di} \leq 0$ , there is no further damage. The healing component reads

$$\dot{\epsilon}_{ij,phs}^h = -\epsilon_{vol} \cdot \left( \frac{\frac{\pi - \theta_R}{6} \cdot \dot{\sigma}_{\perp_1} + \dot{\sigma}_{\perp_2}}{\frac{\pi}{3}} \cdot \frac{1}{fc1} + \frac{F^h}{fs1} + \frac{1}{fh} \right) \cdot \frac{\partial Q_{phs}^h}{\partial \sigma_{ij}} \quad (32)$$

where  $F^h$  is the healing yield criterion,  $Q_{phs}^h$  is the healing potential function,  $\dot{\sigma}_{\perp}$  is the stress rate in the direction perpendicular to the fractures and  $\theta_R$  is the Lode's angle. As can be seen, healing reduces dilatancy. The volumetric strain is now

$$\epsilon_{vol} = \epsilon_1^d + \epsilon_2^d + \epsilon_3^d + \epsilon_1^h + \epsilon_2^h + \epsilon_3^h \quad (33)$$

Finally, the thermomechanical damage-induced permeability changes are modeled with the following empirical function:

$$K_{\parallel} = 10^{\lg(K_0) + \left( \lg(-\epsilon_{vol}) - \lg(-\epsilon_{vol,0}) + 2 \cdot \exp(-f \cdot \sigma_{\perp_2}) \cdot \frac{1}{\ln(10)} (Ei(e^{-\epsilon_{vol}}) - Ei(e^{-\epsilon_{vol,0}})) \right)} \cdot K^* \quad (34)$$

where

$$Ei(x) = \int_{-\infty}^x \frac{\exp(t)}{t} dt = C + \ln|x| + \sum_{i=1}^{\infty} \frac{x^i}{i \cdot i!} \quad (35)$$

Note that  $K^* = 1 \text{ m}^2$ . As can be seen, the secondary permeability depends on the volume variation and the stress state.

In addition, the hydraulically damage-induced permeability changes are modeled using

$$K^s = \begin{cases} 0 & \Delta p_{Fl} \leq \Delta p_{Fl}^{crit} \\ 10^{a+b \cdot \arctan(c \cdot (\Delta p_{Fl} - \Delta p_{Fl}^{crit})) + d \cdot \exp(e \cdot \Delta p_{Fl})} & \Delta p_{Fl} > \Delta p_{Fl}^{crit} \end{cases} \quad (36)$$

In Equation (36),  $\Delta p_{Fl}^{crit}$  is the difference between the pore pressure and the maximum (least negative) principal stress,  $\sigma_3$ .

In total, the Lux/Wolters constitutive model has 45 parameters. However, the number of parameters used in a simulation may be reduced, depending on the phenomena under investigation (e.g., if healing is not considered, the healing parameters are not needed).

## 6. Modeling of an Overpressured Fluid-Injection and Salt-Damage Experiment

In this section, an experiment related to overpressured fluid injection into rock salt is modeled using two TOUGH2-based approaches: (1) a modified version of TOUGH2-EOS9 with pressure-dependent permeability, and (2) a coupled TOUGH-FLAC simulation using EOS4 with stress-dependent permeability. We first conduct the TOUGH2-EOS9 simulation, which is simplified in terms of assuming uniform and constant confining stress in the sample defined by the applied boundary stresses. This model simulation provides us with a starting point for modeling brine damage and provides results for comparison to both the experimental results and the alternative TOUGH-FLAC coupled analysis. We then conduct the TOUGH-FLAC simulation, involving increased complexity, considering spatial distribution of stresses in the sample.

### 6.1 Experimental Set-up and Results

The experiment was conducted by Ralf Wolters in the rock mechanics laboratory of Professor K.-H. Lux at Clausthal University of Technology, Clausthal-Zellerfeld, Germany. In this experiment, a core of rock salt from the Asse salt mine in Germany was used for injection of a fluid containing a fluorescent tracer at a fluid pressure sufficient to cause permeability damage to the rock (Wolters et al., 2012).

As shown in Figure 6, the core was 0.35 m long and 0.15 m in diameter. A fluid-injection chamber 0.1 m in depth and 0.05 m in diameter was drilled into the core.

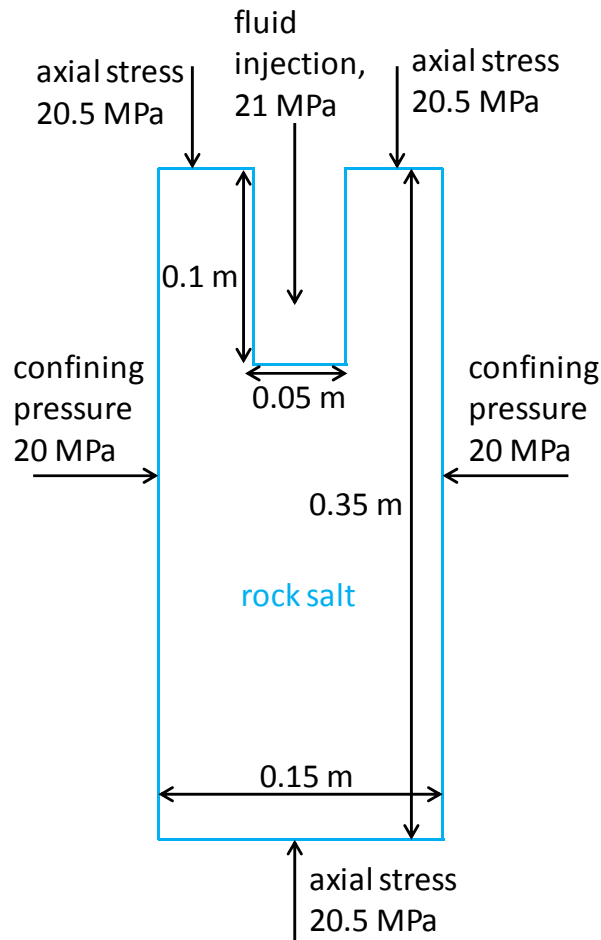


**Figure 6.** Domain diagram for fluid injection into rock salt.

The experiment was conducted in a triaxial cell, with a lateral confining pressure of 20 MPa and an axial stress of 20.5 MPa. Fluid was injected at a pressure of 21 MPa, entering the rock salt through the fluid-injection-chamber surfaces. The fluid pressure at the downstream boundary was maintained at atmospheric pressure (0.1 MPa). Lateral and upper boundaries of the rock salt were no-flow boundaries; flow entered the rock salt exclusively through the fluid-injection chamber.

Observations were made of the resulting fluid volume that infiltrated into the rock salt as a function of time (Figure 7). The experiment was concluded after 6 days of fluid injection at 21 MPa pressure. At the end of the infiltration experiment, the location of the fluid that invaded the salt rock was identified visually by slicing the sample in half (axially) and putting the rock under an ultraviolet light, causing the tracer in the injected fluid to fluoresce (Figure 8).

Under low differential stress and low fluid pressure relative to confining pressure, rock-salt permeability is very low, in fact considered to be effectively zero (Lux, 2009). It has been observed experimentally that when fluid is injected at pressures in excess of the minimum confining pressure, rock salt is damaged and causes the rock-salt permeability to increase, such that fluid infiltration into the rock salt can occur (Lux, 2009).

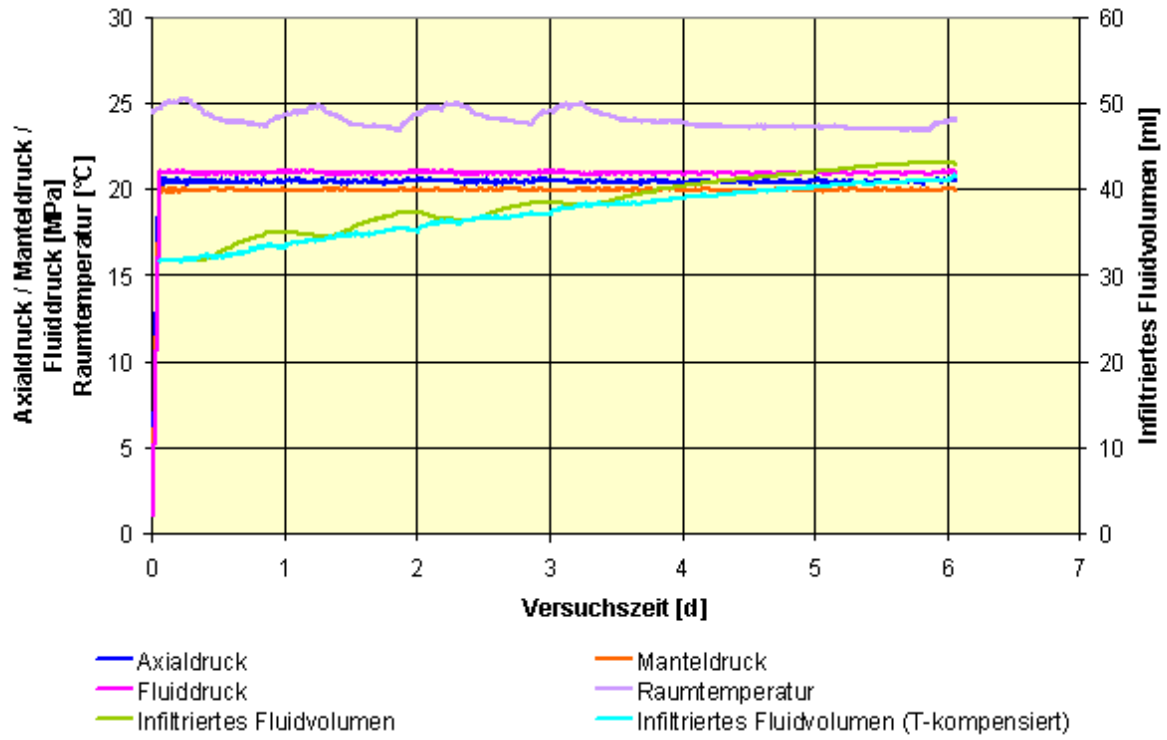


**Figure 7.** Experimental salt infiltration data from Clausthal University showing fluid pressure, stress, temperature, and infiltration volume over 6 days (axialdruck = axial stress, fluiddruck = fluid pressure, infiltriertes fluidvolumen = infiltrated fluid volume, manteldruck = confining stress, raumtemperatur = room temperature, and T-kompensiert= temperature compensated).



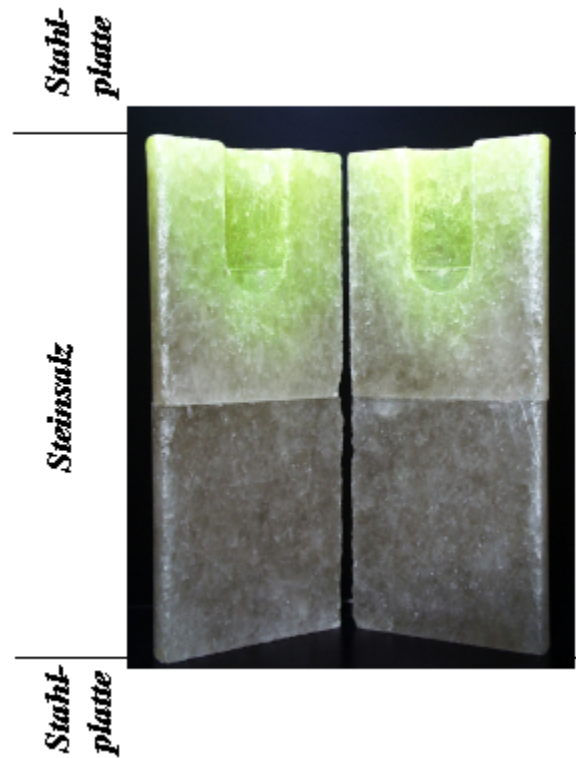


**Figure 8.** Rock salt sample sliced in half showing injection fluid tracer to fluoresce under an ultraviolet light.

## 6.2 TOUGH2-EOS9 Model and Results

A modified version of TOUGH2-EOS9 was used to model the laboratory experiment. This model employs the approximation that mechanical stress within the sample is homogeneous and constant over time, but that fluid pressure is nonuniformly distributed and evolves over time. Thus, variations in the effective stress of the rock can be described in terms of fluid-pressure variations alone. The TOUGH2-EOS9 source code was modified such that the effects of fluid pressure on permeability were included.

The permeability-pressure relationship is based on the Lux/Wolters model,

$$\log(k) = a + b \cdot \arctan\{c(\Delta p_f - \Delta p_c)\} + d \cdot \exp(e\Delta p_f) \quad (37)$$

for  $\Delta p_f > \Delta p_c$ ; otherwise, permeability is not affected by pressure.

The value of  $d$  used was small in magnitude compared with  $a$ ; therefore,  $a$  was taken to be the unperturbed value ( $\Delta p_f = 0$ ) of  $\log(k(m^2)) = -25$ . The other parameters are:  $b = 3.2$ ,

$c = 2.5 \times 10^{-5} \text{ Pa}^{-1}$ ,  $d = 0.05$ ,  $e = 2.0 \times 10^{-6} \text{ Pa}^{-1}$ , where  $\Delta p_f = p_f - p_{\text{min stress}}$ ,  $\Delta p_c = p_c - p_{\text{min stress}}$ ,  $p_f$  is the fluid pressure, and  $p_{\text{min stress}}$  is the lateral confining pressure. The critical pressure for dilatancy,  $p_c$ , is taken to be equal to the minimum confining stress, 20 MPa. The fluid-injection-chamber pressure was set to 21 MPa and was maintained as a constant pressure in the fluid injection chamber. A plot of permeability as a function of pressure is shown in Figure 9. The permeability function displays two regimes that correspond to dilatancy at lower pressures and fracturing at higher pressures. The model calculations in this section are for the dilatancy regime as indicated in Figure 9.

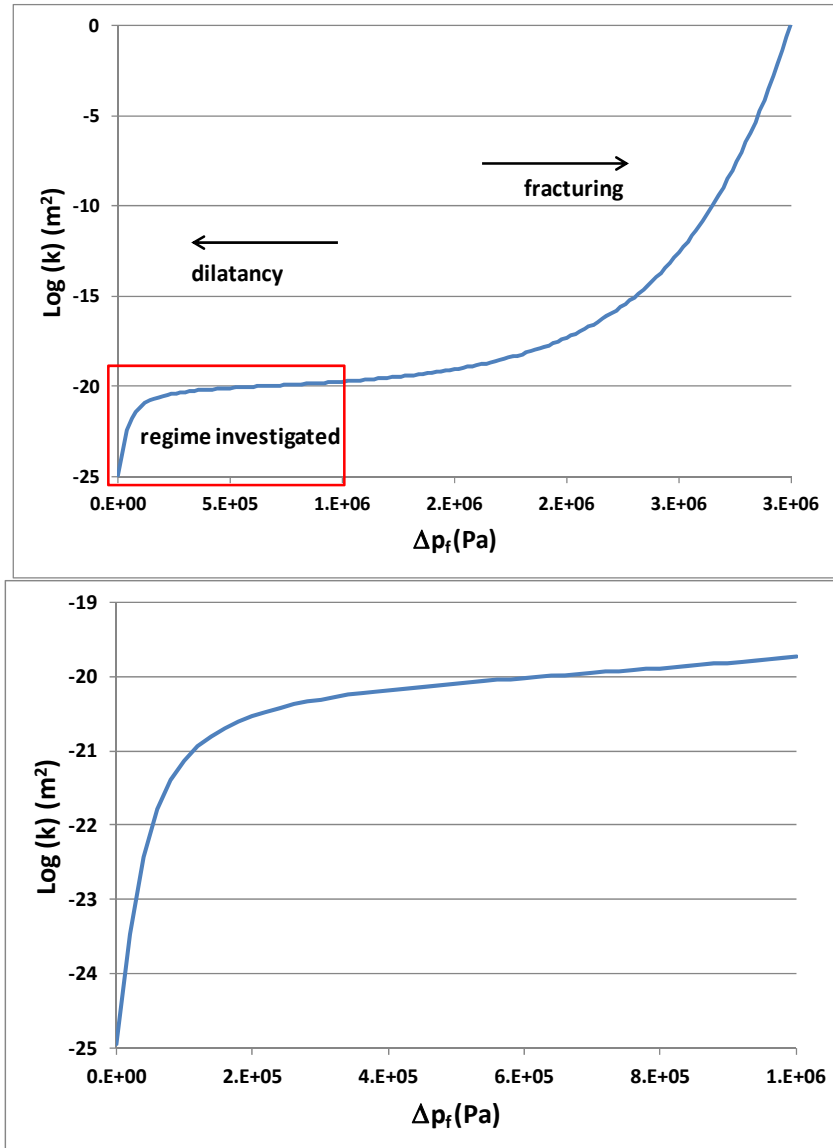


**Figure 9.** Log permeability as a function of  $\Delta p_f$ .

The rock porosity was estimated to be 0.005, based on experimental results for the cumulative volume of fluid injected and the portion of rock invaded. Porosity was kept constant over the duration of the test. The pore compressibility of the rock was assigned a value of zero. The fluid density, viscosity, and compressibility were  $998 \text{ kg/m}^3$ ,  $0.001 \text{ Pa}\cdot\text{s}$ , and  $4.55 \times 10^{-10} \text{ Pa}^{-1}$ , respectively.

Various weighting schemes are possible when computing flow between two grid elements. This is a result of the discrete nature of numerical flow solutions and the fact that permeability is treated as a property associated with a pair of adjacent grid elements, rather than the property of an individual grid element. For this calculation, mobilities were upstream weighted, and permeabilities were harmonically weighted. This weighting is a compromise between full upstream weighting for both mobility and permeability, as recommended for transient unsaturated flow, and harmonic weighting of permeability for single-phase flow (Pruess et al., 2011). The permeability modification was upstream weighted, i.e., the highest pressure for any adjacent pair of grid elements was used to modify both permeabilities for the pair according to Equation (37).

The observed fluid infiltration over time was found to have a large quantity of fluid infiltrate the sample in the first hour of the test. In this case, we interpreted that could be a feature of the damage zone around the chamber drilled for fluid injection. This damage zone was taken to be a 0.01 m thick band around the chamber's radial perimeter and along the base of the chamber. The damage zone was assigned properties of  $\log(k) = -24$  and porosity of 0.151. These parameters were assigned based on comparisons between computed results and experimental observations.

Relative permeability and capillary-pressure functions were needed, because the rock is initially unsaturated, with a nominal saturation of  $1 \times 10^{-9}$ . The relative permeability,  $k_r$  function for the liquid was assigned to be a linear function of liquid saturation ( $S$ ),  $k_r = S$ . The capillary pressure was assigned a value of zero for all liquid saturations.

The 0.075 m radius, 0.35 m long rock was modeled as a 2-dimensional radial, R-Z system with grids spaced radially every 0.005 m and vertically every 0.01 m. The chamber for fluid injection was 0.025 m radius and 0.10 m long space that was represented by one element. A total of 477 nodes were used.

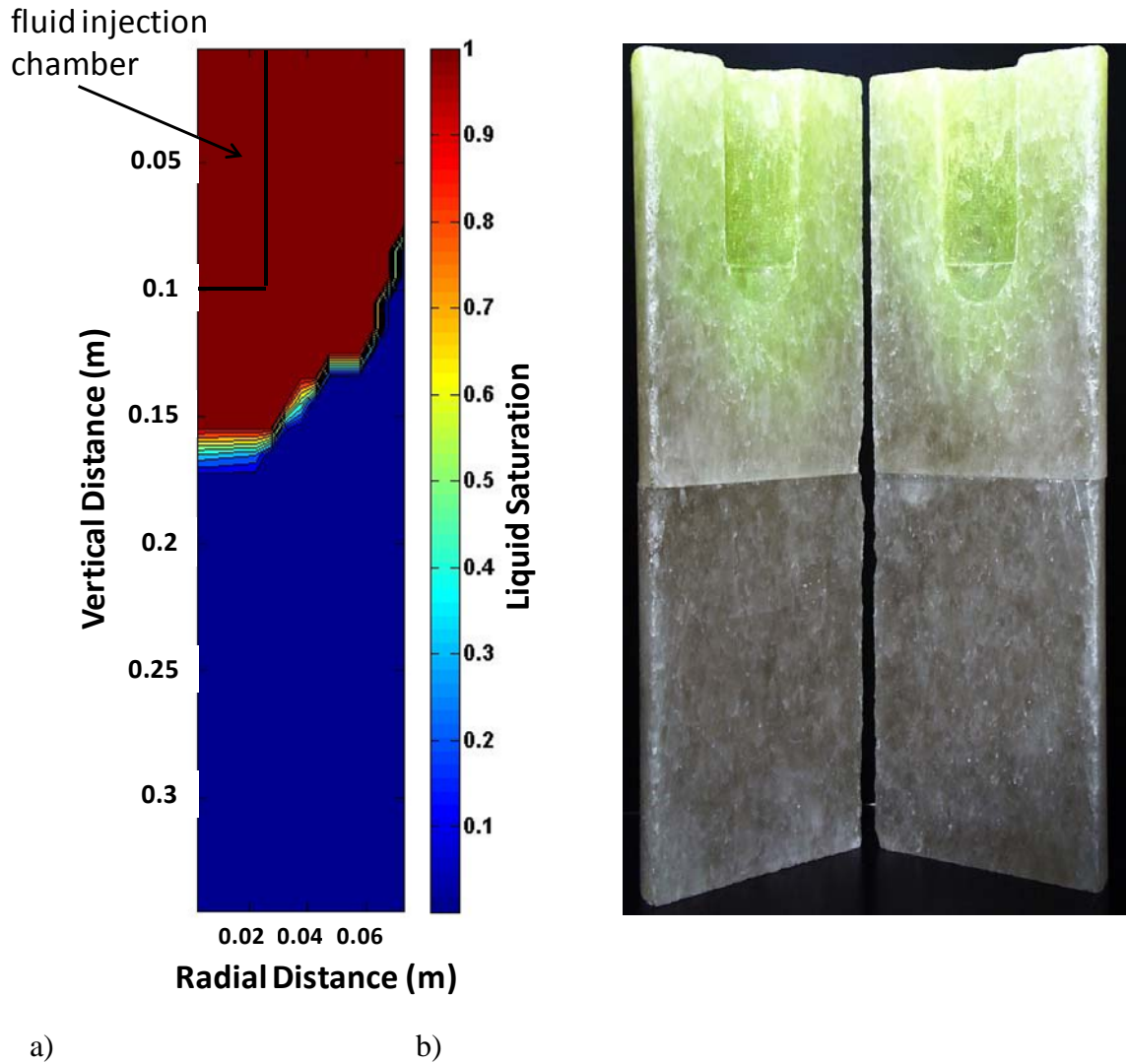


**Figure 10.** Saturation profiles at 6 days (a) Saturation computed using modified TOUGH2-EOS9; (b) fluorescent green dye pattern from rock salt fluid-injection experiment.

Figure 10a displays the results for the saturation of the injected phase after 6 days. The reddish-brown color represents complete saturation; the dark blue represents a saturation of  $10^{-9}$ . The black outline identifies the chamber for fluid injection. This can be seen to be qualitatively similar to the experimental results shown in Figure 10b.

Figure 11 shows the cumulative recovery computed by the model compared with the experiment.

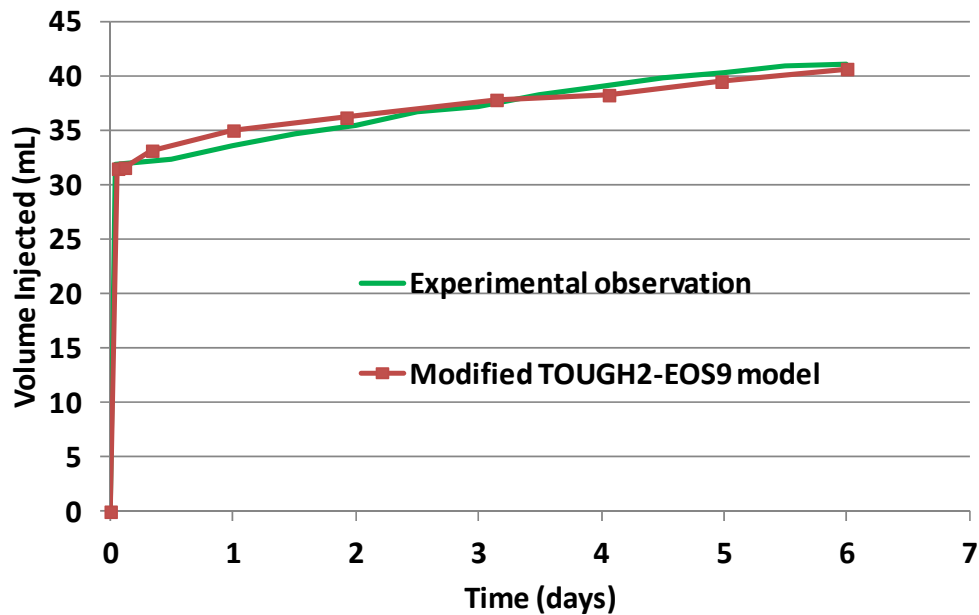


Figure 11. Cumulative injected fluid as a function of time.

The damage zone around the fluid-injection chamber receives most of the initial fluid volume entering the sample during the first hour of the test, about 29.6 mL out of the initial 32 mL. After about 8 hours, the calculated response has caught up with the experimental observation. The last 9 mL of the injected fluid proceeds to enter the sample at a much slower rate over the remainder of the 6-day test.

### 6.3 TOUGH-FLAC EOS4 Model and Results

In this section, we present TOUGH-FLAC modeling of the experiment using the EOS4 equation-of-state module. The EOS4 module can model full multiphase processes involving gas and liquid phases with air and water components, as well as salinity; this is the module that would be applicable to study high-temperature coupled processes associated with a high-level nuclear waste disposal in salt. The model simulations using EOS4 are much more computational demanding than when using EOS9. In this simulation example, up to 1000 time steps were required when using EOS4, whereas single-phase flow simulations with EOS9 required less than 50 time steps.

The TOUGH-FLAC model grid has 856 elements (about twice the number of elements as in the previous TOUGH2-EOS9 model) and included the steel plates above and below the sample as well as the fluid injection chamber. We used the same material parameters as in the previous TOUGH2-EOS9 simulation, including the same equation and parameters for permeability change caused by the overpressure. However, we employed a different approach for capturing the initial sharp increase in injection volume. In this model, we did not assign a damage zone to the wall of the injection chamber, but considered that this initial volume could be caused by compressibility effects along the pipes in the injection system between flow gauge and the

injection chamber. We considered this by explicitly modeling fluid flow through the injection pipe and injection chamber, considering compressibility effects; we assigned rock compressibility to the injection chamber that was calibrated to achieve the appropriate initial volume increase. Moreover, we also used a slightly different approach for calculating the pressure-induced changes in permeability; we first corrected permeability for overpressure locally at each individual element, and then we used the standard TOUGH2 permeability evaluation at each connection. We used upstream weighting for permeability correction, which is conceptually equivalent to the approach used in the TOUGH2-EOS9 simulation, given an initially homogenous permeability.

The main difference in using a coupled TOUGH-FLAC simulation compared to that of a TOUGH2-EOS9 simulation is that the stresses are no longer necessarily homogenous within the sample. In fact, it has been observed in previous experiments and models of these types of tests that the stress can locally be much lower than the confining boundary stress—which could significantly impact fluid infiltration (Wolters et al., 2012). Near the upper steel plate, a much quicker infiltration can occur because of stress redistribution from the rock-salt sample to the steel plate (Wolters et al., 2012). To investigate such an effect in detail, we conducted two types of simulations with TOUGH-FLAC:

- 1) A simulation in which the stress in the rock salt is assumed homogenous and equal to the applied confining stress (simplified stress analysis)
- 2) A simulation in which the stress redistribution in the rock sample is fully accounted for (full stress analysis).

The results of these analyses compared with the measured data are shown in Figure 12. The results show an increased rate of injection in the case of a full stress analysis, especially in the first few days. In general, the simple stress analysis shows a better fit with the experimental data during the first few days. The good fit for the simple stress analysis is consistent with the previous modeling results using TOUGH2-EOS9. The match to the experimental data will depend on the parameters assigned to the permeability-pressure relationship in Equation (37), and would need to be recalibrated for the full stress analysis.

Figures 13 and 14 illustrate the difference in infiltration rate for the simple stress analysis (Figure 13) and the full stress analysis (Figure 14). The results show that in the case of the full stress analysis (Figure 14), the fluid penetrates the sample at a much higher rate than in the case of simple stress analysis (Figure 13), especially near the top of the sample. In the case of the simple stress analysis, it takes 3 to 4 days for the fluid to reach the lateral boundary of the sample, whereas it takes less than 1 day in the case of the full stress analysis. A rapid fluid infiltration near the top of the samples has been frequently observed in laboratory tests (Ralf Wolters, personal communication, August 2012) and is also discussed in Wolters et al. (2012). The reason for the increased fluid-infiltration rate at the upper part of the sample is that the stress is affected by the upper (stiff) steel plate. Indeed, Figure 15 shows that the least compressive principal stress in that region is much less than the confining stress, i.e., much less than 20 MPa. (Note that the value -20 MPa shown in Figure 15 signifies compressive stress.) The least compressive principal stress is as low as 10 MPa just below the upper steel plate, leading to an overpressure of about 10 MPa in that region.

Based on these results, we conclude that we have tested the use of TOUGH-FLAC and the Lux/Wolters model related to forced fluid injection into salt. However, further sensitivity studies and comparison to experimental data should be done to increase understanding of the underlying processes occurring in the experiment, including stress-dependent porosity changes that would likely occur along with the pressurization of the rock-salt sample.

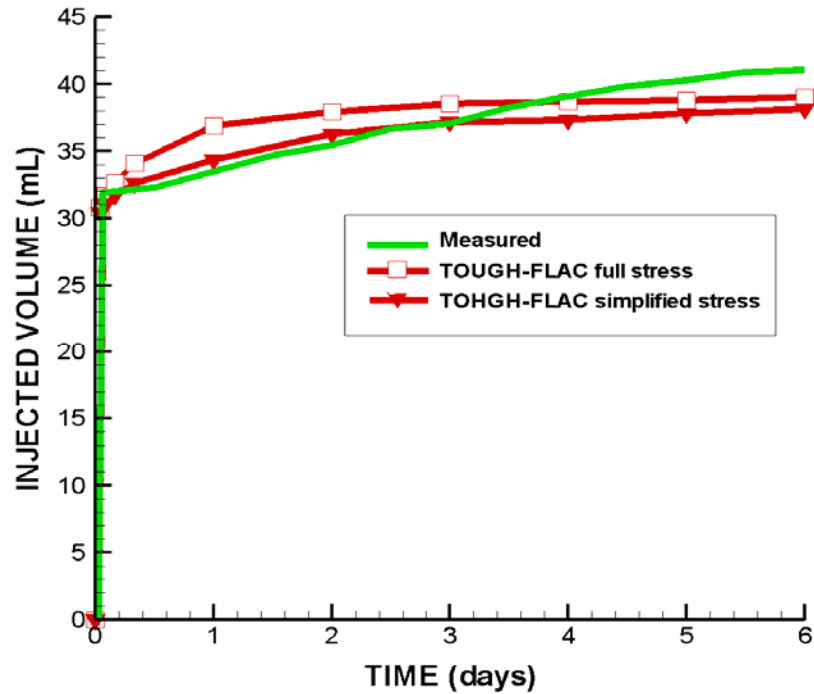


**Figure 12.** Injected fluid volume as a function of time with comparison of TOUGH-FLAC full stress analysis with that of TOUGH-FLAC simplified stress analysis.

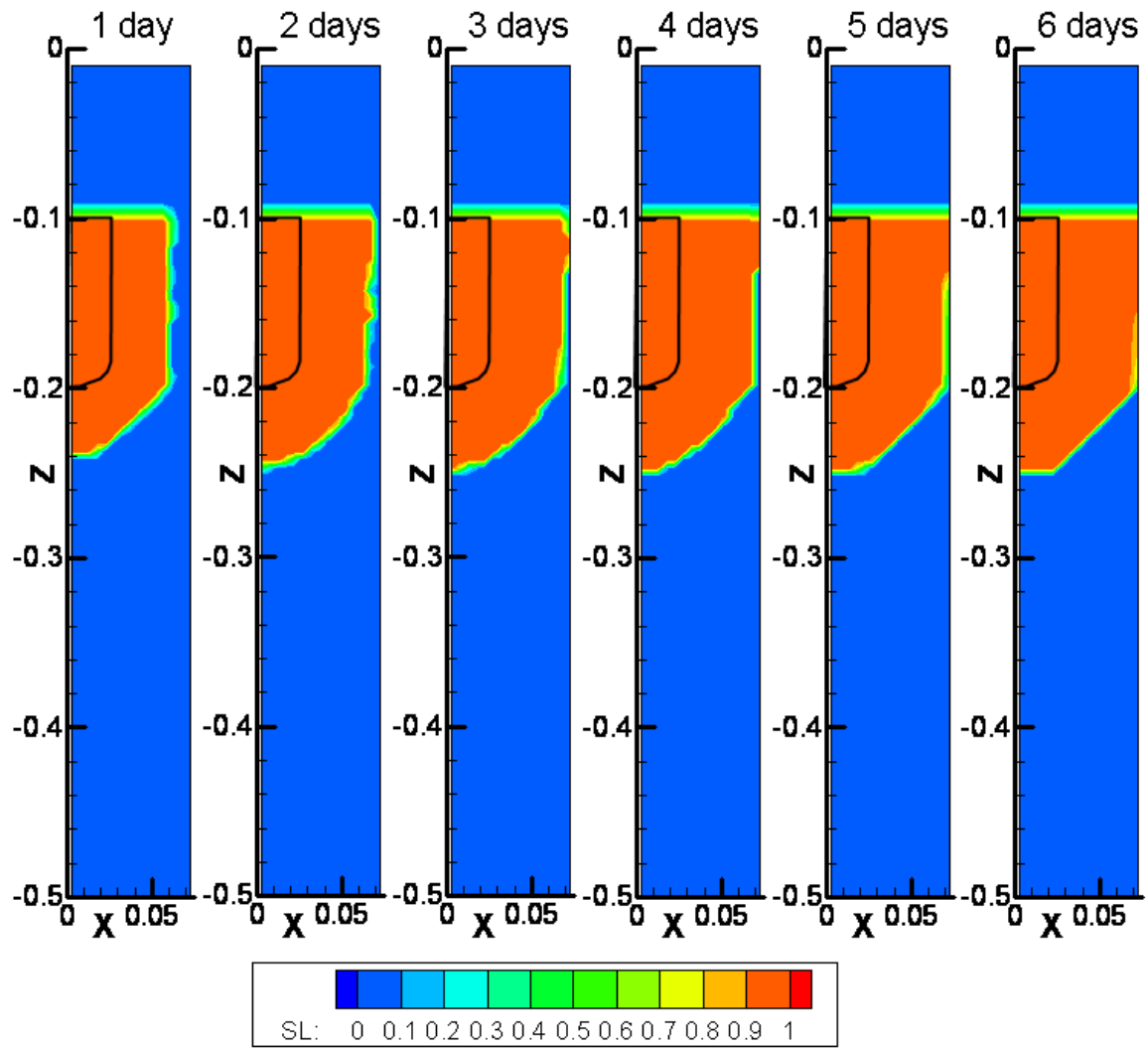
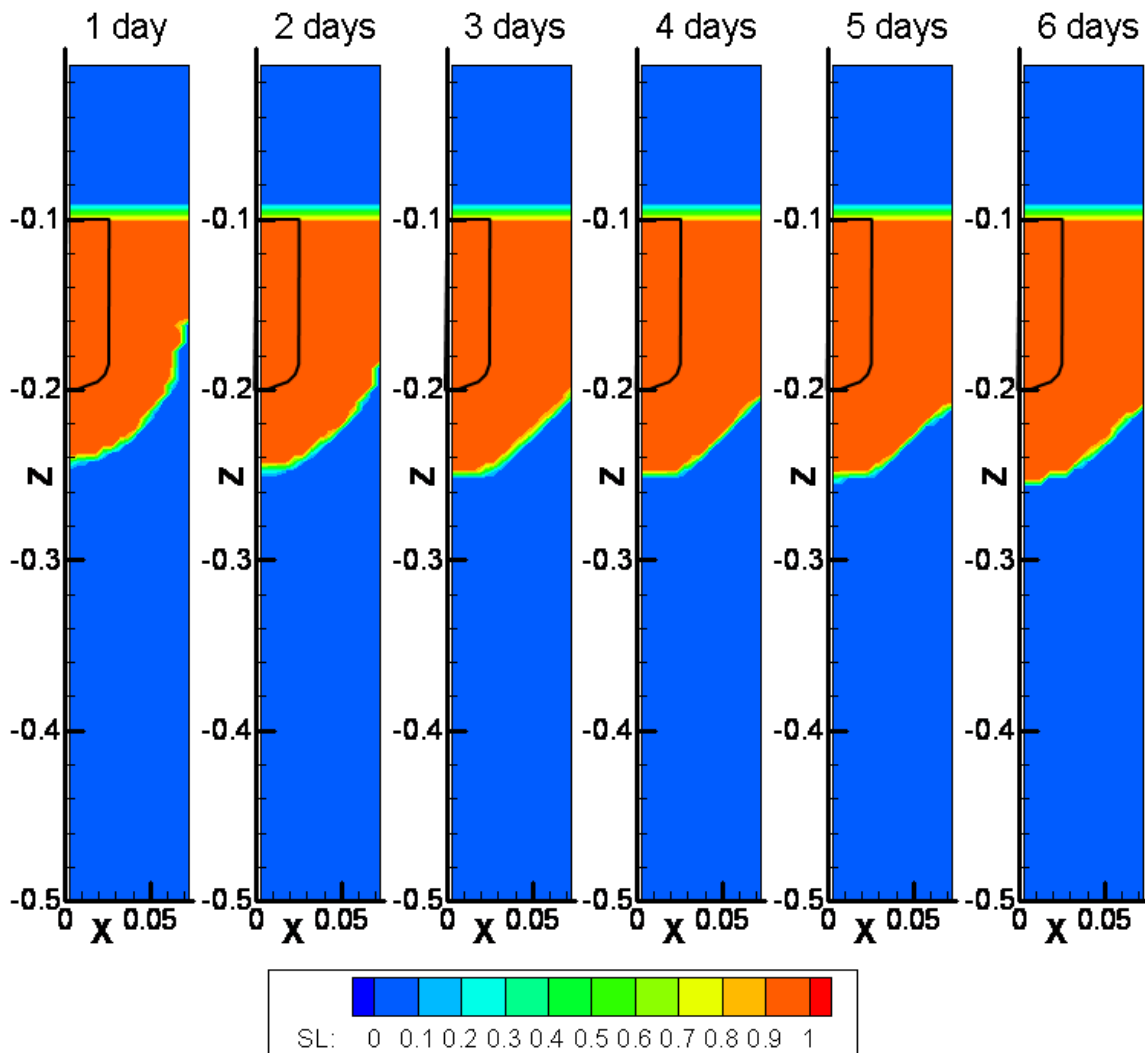
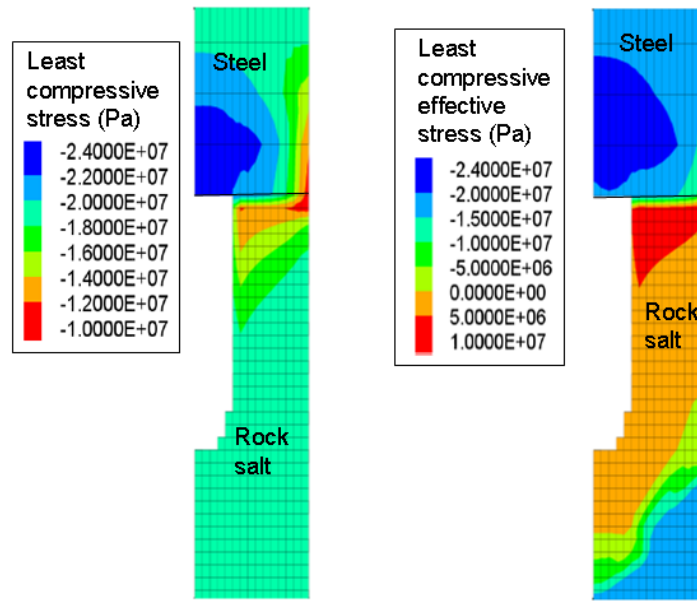


Figure 13. Evolution of fluid liquid saturation in the case of TOUGH-FLAC simple stress analysis.





**Figure 14.** Evolution of fluid liquid saturation in the case of TOUGH-FLAC full stress analysis.



**Figure 15.** Distribution of (a) least compressive principal stress and (b) least compressive effective stress at 6 days.

## 7. FLAC3D Simulation Using the Lux/Wolters Model and the Large-Strain Mode

The constitutive model Lux/Wolters developed by Clausthal University of Technology and described in this report has been used to simulate the long-term behavior of a storage cavern excavated in rock salt. The geometry of the model is shown in Figure 16. The cavern has a length of 100 m and a radius (at the central part) of 20 m. The initial volume of this cavern is about  $1.80 \times 10^5 \text{ m}^3$ .

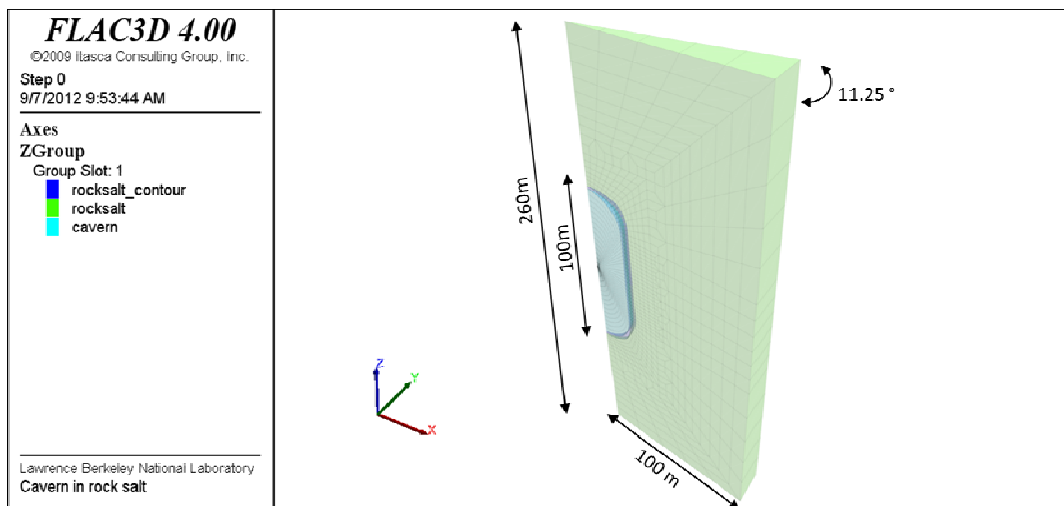


**Figure 16.** Geometry of the model and zones defined for a rock-salt cavern.

The model consists of a wedge that spreads  $11.25^\circ$  across the  $X$  axis, with the axis in the middle. The length of the model along this axis is  $100 \cdot \cos(11.25/2^\circ)$  m. In the  $Z$  direction, the model extends from -120 m to -380 m. The uppermost point of the cavern is at  $Z=-200$  m. In total, the grid is composed of 1604 zones and 3179 gridpoints. Most of these zones correspond to the cavern, and will be therefore deactivated as the excavation occurs. The rock salt around the cavern is modeled by 764 zones.

In the simulation conducted, it has been assumed that the overburden is composed entirely of rock salt. The stress due to this overburden has been applied on top of the model, at  $Z=-120$  m. In addition, the initial stress field is assumed to be isotropic, because of the creeping process of the rock-salt formation over time. Regarding the boundary conditions, the velocities of the boundary gridpoints have been set equal to zero in the directions where some surrounding ground is present. Because of the significant amount of deformation expected, the numerical simulation has been conducted using FLAC3D's large strain mode. In this mode, the coordinates of the gridpoints are updated and the volume of every zone is calculated with these new coordinates, but the numerical procedure is the same as in the small strain mode.

In the simulation we adopted parameters for the Lux/Wolters model corresponding to a parameter set used and presented in Wolters et al. (2012).

The simulation is conducted in three steps:

1. The initial and boundary conditions are applied to the model;
2. The cavern excavation is modeled. To do so, FLAC3D's null model is assigned to the cavern zones. This way, the stresses within the cavern are equal to zero;
3. The creep model is activated in the third step. The rock salt is left to creep until the desired creep time limit is reached. During this period, no pressure is applied to the cavern surface, which represents the worst possible scenario. In the current simulation, a creep time of 100 years has been set.

The results of the simulation are shown below. Figure 17 displays the equivalent Von Mises stress obtained. This figure shows that the maximum stress is not attained at the cavern surface, but within the rock mass, several meters from the cavern perimeter. In fact, at the cavern surface, the stress decreases as a result of stress rearrangements that occur as a result of the loosening (i.e., damage) of the rock mass and the intensified creep rate. This is one of the features that characterizes the Lux/Wolters model.

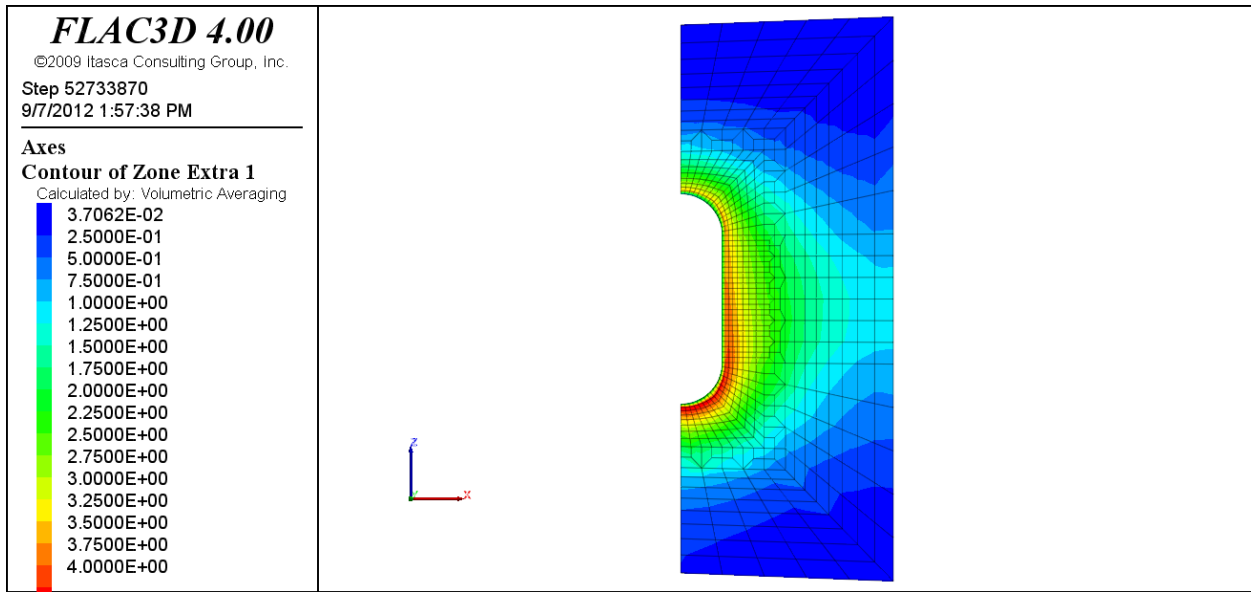


**Figure 17.** Von Mises equivalent stress distribution obtained after 100 years.

Figure 18 displays the magnitude of displacement. As can be seen, the maximum convergence is attained along the central part of the cavern. According to these results, a maximum displacement of about 3 cm is expected after 100 years of creep (without internal pressure). The overall convergence of the cavern is 0.28 % (Figure 19).

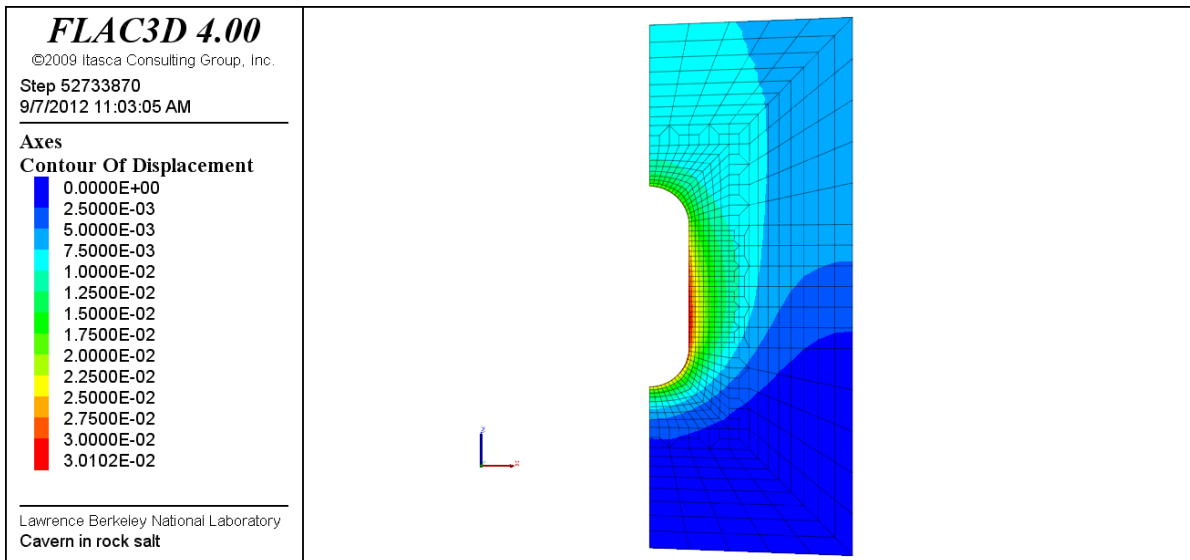


**Figure 18.** Contour of displacement (in meters) around the cavern after 100 years.

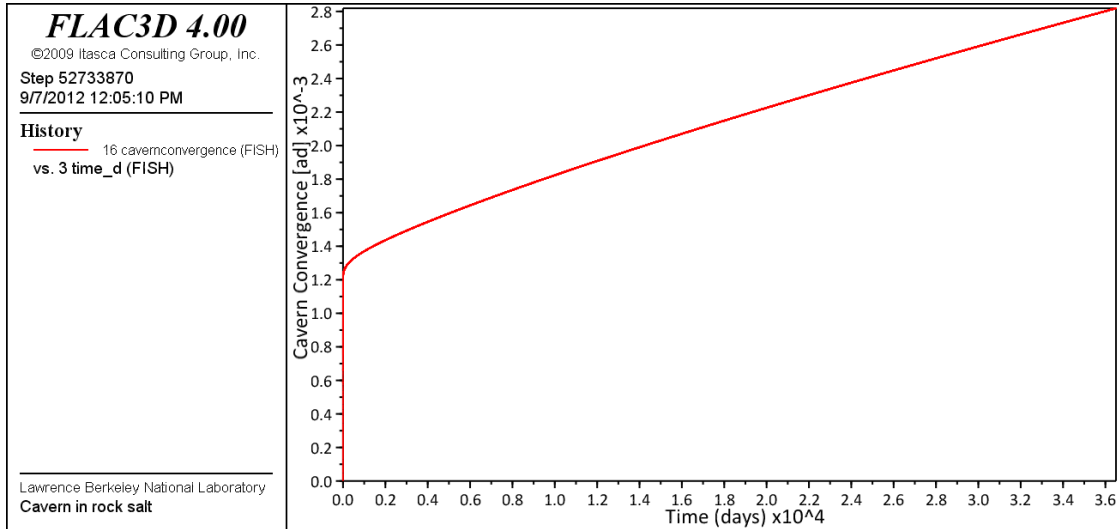


Figure 19. Evolution of cavern convergence over time.

In order to reach greater values of convergence, the simulated time should increase considerably, leading to longer calculation times. In Figure 20, the magnitude of displacement obtained after a creep time of 100,000 years is shown. As it can be seen, the displacement along the cavern contour exceeds 4 m. The overall convergence of the cavern is now about 38 %, and its shape has slightly changed.

Finally, we recognize that the deformation expected when using creep models (particularly in the case of long-term calculations) will require simulations using the large strain mode. As mentioned above, in order to conduct coupled TOUGH2 and FLAC3D simulations using the large strain mode, the TOUGH2 mesh must be updated along with the deformation of the FLAC3D mesh. This will be addressed in the near future.

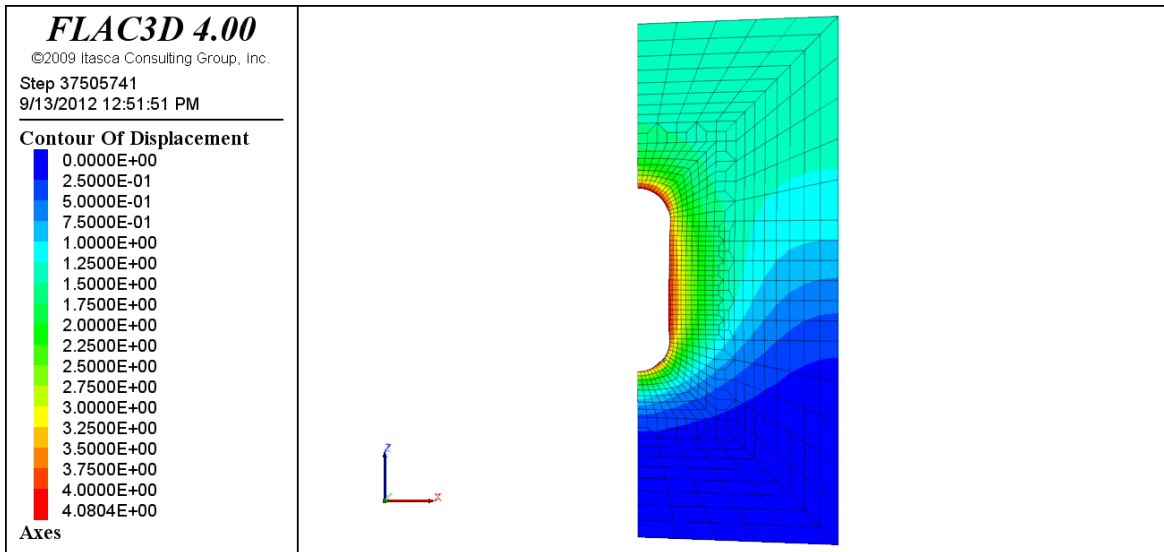
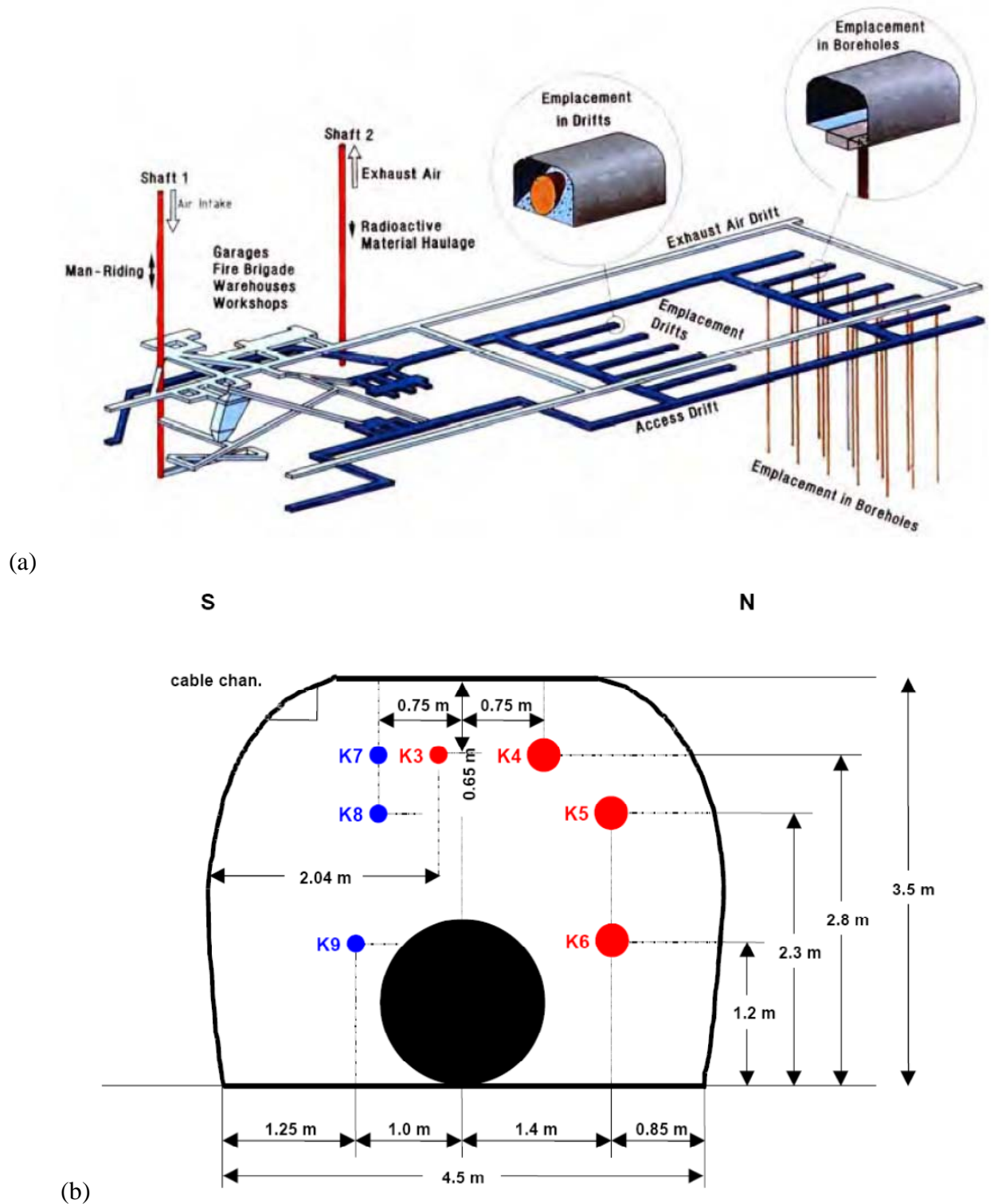


Figure 20. Contour of displacement (in meters) around the cavern after 100,000 years.

## 8. Generic Salt-Based Repository Model for THM Analysis

In this section, we present a simulation of a generic repository case assuming an EBS design with waste emplacement in horizontal tunnels backfilled with crushed salt. We adopt a repository design following the German repository concept in salt with detailed drift geometry from the thermal simulation of drift emplacement (TSDE) *in situ* test carried out in the Asse salt mine, Germany (Figure 21). We intend to use this generic repository model for testing TOUGH-FLAC and the Lux/Wolters model over a 100,000 year time period, including high-temperature effects, creep convergence, large strain, damage and permeability evolution with potential water infiltration. The results presented in this report are related to an initial scoping calculation of the heat load and thermally-driven multiphase fluid flow responses without consideration of geomechanical effects.

For our generic-model-simulation example, we assume a repository located at a depth of 600 m in a bedded salt layer that is 400 m thick. We used the German design for a waste package, 5.5 m long, 1.6 m in diameter, emplaced on the floor of the tunnels with a gap of 3 m between individual waste packages. We represent the problem in a 2-D vertical cross-section, using a half symmetric model that extends up to the ground surface and down 600 m below the tunnel (Figure 22). We use the heat load developed within the UFD as a Generic Disposal System Environment (GDSE) for Pressurized Water Reactor (PWR) used nuclear fuel based on 17x17 fuel rod array assembly design data with 0.47 MT per assembly and 60 GWd/MT burn-up (Carter et al., 2011). We use the heat load for 10 PWR assemblies in the waste package assuming emplacement 20 years from the time out of reactor, leading to an initial heat load of 8499 W per waste package. For the assumed canister spacing we then calculate an initial line load per meter tunnel of  $8499/8.5 = 1000$  W/m.



**Figure 21.** (a) Typical layout of a high-level waste repository in salt including emplacement in horizontal tunnels, and (b) cross-section from the TSDE *in situ* heater experiment at Asse mine (Bechthold et al., 2004).

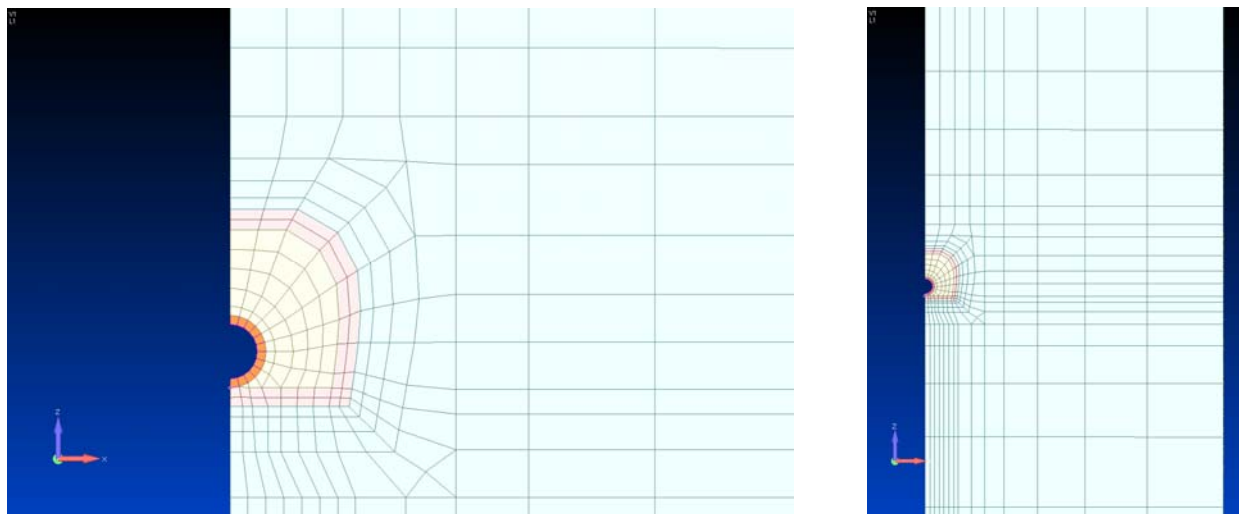


**Figure 22.** 2-D model grid for modeling of a horizontal nuclear waste emplacement tunnel in salt with the dimension of the waste package and tunnel given in Figure 21.

We conducted this initial scoping calculation using salt backfill at 35% porosity, being at an initial water saturation of 1%, whereas the surrounding rock salt has a porosity of 1% and being fully saturated at hydrostatic fluid pressure. We adopted typical properties for rock salt and crushed backfill extracted from the 2011 GDSM report (Clayton et al., 2011), the Generic Repository Design Concepts and Thermal Analysis report (Harding et al., 2011), as well as from investigations at the Asse mine, TSDE heater experiment (Bechthold et al., 2004). The thermal conductivity of the solid rock salt was set to 4 W/m $\cdot$ °C, whereas the thermal conductivity of the porous backfill was set to 2 W/m $\cdot$ °C at full saturation and 0.6 W/m $\cdot$ °C at dry conditions. The permeability of the rock salt was set to  $1 \times 10^{-22}$  m $^2$ , whereas the permeability of the backfill was set to  $1 \times 10^{-11}$  m $^2$ . For the water retention and relative permeability functions (which are not well known for salt), we selected functions that should be representative for low permeability and low porosity medium in the case of solid rock salt and a function representing high porosity and high permeability medium for the crushed salt backfill. We used the capillary pressure model due to van Genuchten (1980) with the capillary scaling parameter  $P_0$  set to 14.7 MPa and 3.3 kPa, respectively for solid rock salt and crushed salt backfill.

Figure 23 presents the calculated evolution of temperature, water saturation and fluid pressure. As mentioned, in this report we present results without considering geomechanical effects. Over the longer term geomechanical effects, including convergence and compaction of the backfill will significantly impact the THM evolution, especially within the backfill. However, over the first few tens of years our results might be quite representative. For example, at the Asse mine heater experiment, the tunnel converged with a compression of the crushed backfill from 35% to 25% porosity in 8 years. This means that still after 8 years a substantial porosity and permeability remains in the backfill. In our simulations we achieved a peak temperature of 226 °C after 8 years in the backfill near the surface of the heat releasing waste package (Figure 23a). The temperature near the tunnel wall peaks at about 130°C after about 40 years.



Figure 23b shows that the backfill stays dry at a low liquid saturation, except very close to the host rock where we can observe some saturation increase over the longer term. However, if we consider the tunnel convergence and compaction of the crushed salt, the saturation evolution could be completely different after a few hundred years as the backfill might compact to a porosity approach 1% and thereby leading to fully saturated conditions with increasing pressure as fluid is squeezed within the pores.

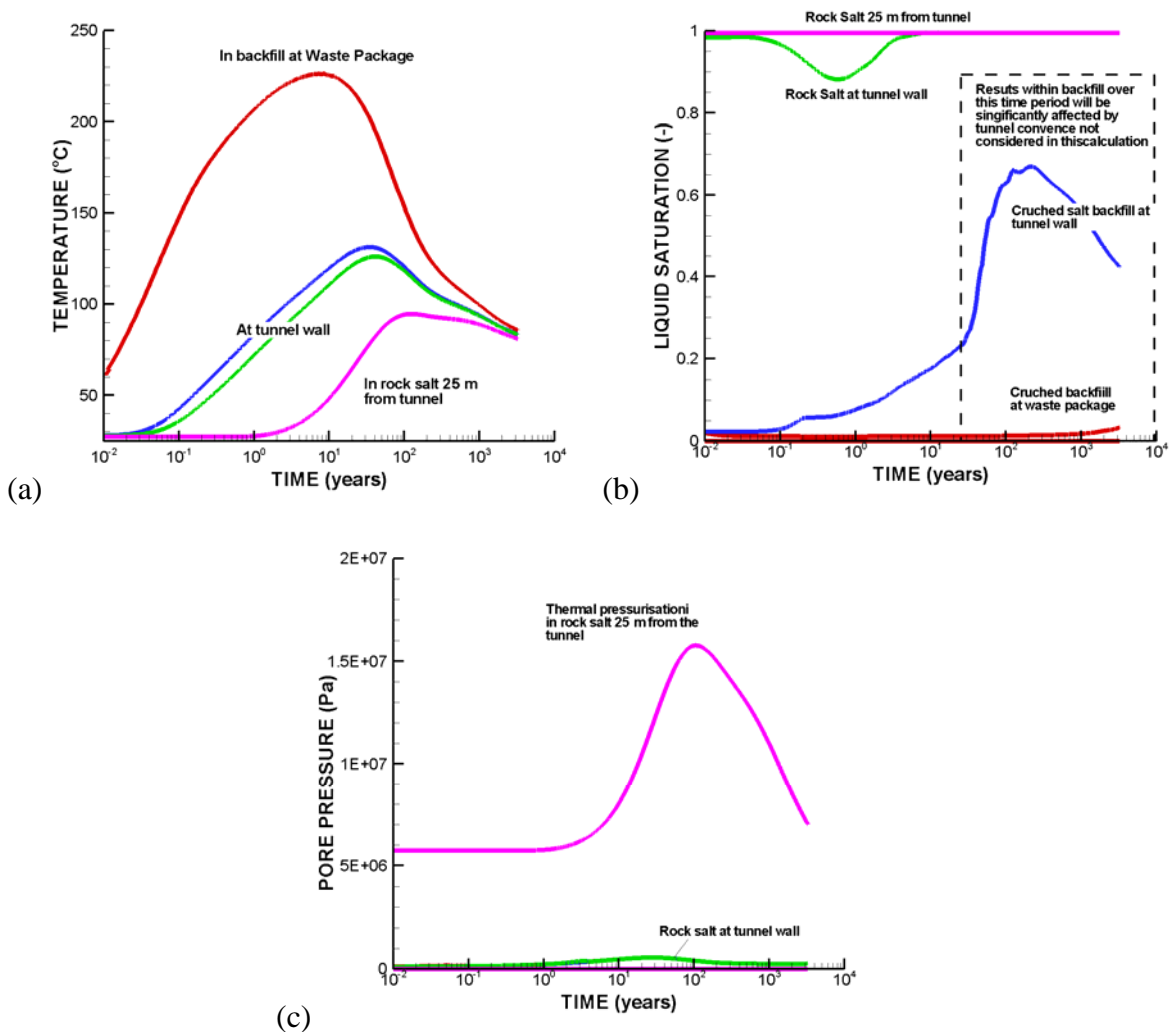


**Figure 23.** TOUGH2 simulation results of the evolution of (a) temperature, (b) liquid saturation and (c) pore pressure.

In Figure 23c we can observe a significant thermal pressurization in the rock salt 25 m away from the tunnel, a phenomenon that has been observed *in situ* when low permeability geological media are heated up. In this case, for the assumed rock salt permeability of  $1 \times 10^{-22} \text{ m}^2$  and a pore compressibility of  $3 \times 10^{-9} \text{ Pa}^{-1}$  we observe a significant pressure increase up to 15 MPa, a pressure that could be close to or exceed the lithostatic stress at a depth of 600 m. This could lead to

increased fluid infiltration and fracturing analogous to the above laboratory study on forced fluid infiltration caused by overpressure.

Overall, the simulation presented in this section demonstrates the applicability of the TOUGH2 for simulating high-temperature multiphase flow processes at a salt based repository. The next step will be to extend the simulation to a coupled TOUGH-FLAC analysis, gradually including more complex processes such as creep and large deformations along with development and testing of such features in the TOUGH-FLAC simulator.

## 9. Conclusions

In FY2012, LBNL's work aimed at exploring and demonstrating the capabilities of the current modeling tool (TOUGH-FLAC) for modeling of temperature-driven coupled flow and geomechanical processes in salt. This includes exploring and developing necessary key features required for such modeling and testing against relevant information related to water fate and transport in published experimental data. We conclude that with some additional developments, the TOUGH-FLAC combination can provide the necessary modeling tool for modeling coupled processes associated with disposal of high-level in salt formations, including high-temperature multiphase flow and transport processes, coupled with time-dependent geomechanical (creep) processes, including large deformations.

Our collaboration with Professor Lux and his group at Clausthal University in Germany has been extremely useful, with hands-on collaboration on the development and application of coupled FLAC<sup>3D</sup> and TOUGH2 simulations for modeling salt coupled geomechanical processes. Through our collaboration, we have access to an advanced constitutive model that has been continuously developed since the early 1980s and includes key features for modeling coupled THM processes and their impact on permeability, water flow, and transport. We have successfully adopted and applied TOUGH-FLAC and the Lux/Wolters model to simulation examples related to forced-water infiltration in rock salt and cavern creep deformations. Moreover, we have demonstrated the applicability of TOUGH2 to simulate high-temperature multiphase flow processes associated with a salt-based nuclear waste repository.

The next step will be to develop and test an algorithm for coupling TOUGH2 and FLAC3D, including strong pore-volume coupling under large strain and deformation, and to develop appropriate coupling algorithms for time-dependent (creep) behavior. Then, in FY2013, we intend to continue our collaboration with Professor Lux and his group at Clausthal University by continued testing of constitutive models for the damage evolution of salt and its impact on brine migration, also adding high-temperature effects. The new capability will be tested by modeling existing brine migration laboratory experiments and *in situ* heater tests, such as those at the Asse salt mine, Germany. Moreover, we will simulate high-temperature-driven coupled effects around a generic repository tunnel, to study the evolution of permeability and water flow.

## 10. Acknowledgements

Funding for this work was provided by the Used Fuel Disposition Campaign, Office of Nuclear Energy, of the U.S. Department of Energy under Contract Number DE-AC02-05CH11231 with Lawrence Berkeley National Laboratory.

## 11. References

- Bechthold W., E. Smailos, S. Heusermann, W. Bollingerfehr, B. Bazargan Sabet, T. Rothfuchs, P. Kanlot, J. Grupa, S. Olivella, and F.D. Hansen, 2004. Backfilling and sealing for radioactive waste in salt (BAMBUS II project). European Commission Report, EUR 20621.
- Carter, J., A. Luptak, and J. Gastelum, 2011. Fuel cycle potential waste inventory for disposition. FCR&D-USED-2010-000031, Rev. 4. October, 2011.
- Claytone et al., 2011. Generic Disposal System Modeling—Fiscal year 2011 progress report. FCRD-USED-2011-000184, August, 2011
- Hampel A. et al., 2010. Benchmarking of geomechanical constitutive models for rock salt. American Rock Mechanics Association, ARMA 10-287, 44<sup>th</sup> US Rock Mechanics Symposium, Salt Lake City, Utah, June 27-30, 2010.
- Hardin, E., H. Greenberg, M. Sutton, M. Fratoni, J. Carter, M. Dupont, R. Howard, 2011. Generic Repository Design Concepts and Thermal Analysis (FY11). SAND2011-6202. August, 2011.
- Hermann W., W.R. Wawersik and H.S. Lauson, 1980. Analysis of Steady State Creep of Southeastern New Mexico Bedded Salt, Sandia National Laboratories, SAND80-0558.
- Hermann W., W.R. Wawersik and H.S. Lauson, 1980. Creep Curves and Fitting Parameters for Southeastern New Mexico Rock Salt, Sandia National Laboratories, SAND80-0087.
- Itasca, 2009. FLAC3D, Fast Lagrangian Analysis of Continua in 3 Dimensions, Version 4.0. Minneapolis, Minnesota, Itasca Consulting Group, 438pp.
- Kachanov, L., 1986. Introduction to Continuum-Damage-Mechanics. Martinus Nijhoff.
- Kim J., E. Sonnenthal, and J. Rutqvist, 2012. A modeling and sequential numerical algorithms of coupled fluid/heat flow and geomechanics for multiple porosity materials. International Journal of Numerical Methods in Engineering (accepted Feb, 2012).
- Lux, K., 1984, Gebirgsmechanischer Entwurf und Felderfahrung im Salzkavernenbau: Ein Beitrag zur Entwicklung von Prognosemodellen für den Hohlraumbau im duktilen Salzgebirge. Stuttgart: Ferdinand Enke Verlag.
- Lux, K.-H., 2009, Design of salt caverns for the storage of natural gas, crude oil and compressed air: Geomechanical aspects of construction, operation and abandonment, from: Evans, D. J. & Chadwick, R. A. (eds) Underground Gas Storage: Worldwide Experiences and Future Development in the UK and Europe. The Geological Society, London, Special Publications, 313, 93–128.
- Minkley W and Popp T. 2010. Final Disposal in Rock Salt- Geomechanical Assessment of the Barrier Integrity. Proceedings of the 44th U.S. Rock Mechanics Symposium, Salt Lake City, Utah, USA, June 27-June 30, 2010: American Rock Mechanics Association ARMA, Paper No. 492. Popp T., Kern, H., Schulze O. 2001. Evolution of dilatancy and permeability in rock salt during hydrostatic compaction and triaxial deformation. Journal of Geophysical Research, Vol. 106, No. B3, Pages 4061-4078, March 10, 2001.

- Norton F.H., 1929. Creep of Steel at High Temperatures. New York: McGraw-Hill Book Company.
- Popp T. and Minkley W. 2010. Salt barrier integrity during gas pressure build-up in a radioactive waste repository – Implications from lab and field investigations. Proceedings of the 44th U.S. Rock Mechanics Symposium, Salt Lake City, Utah, USA, June 27-June 30, 2010: American Rock Mechanics Association ARMA, Paper No. 492.
- Popp, T., H. Kern, and O. Schulze, 2001. Evolution of dilatancy and permeability in rock salt during hydrostatic compaction and triaxial deformation. *Journal of Geophysical Research*, 106, 4061-4078.
- Pruess, K., C. Oldenburg, and G. Moridis, 2011. TOUGH2 User's Guide, Version 2, Lawrence Berkeley National Laboratory report LBNL-43134 (revised).
- Rutqvist, J., 2011. Status of the TOUGH-FLAC simulator and recent applications related to coupled fluid flow and crustal deformations. *Computational Geosciences*, 37, 739–750.
- Rutqvist, J., Y. S. Wu, C.- F. Tsang, and G. Bodvarsson, 2002. A Modeling Approach for Analysis of Coupled Multiphase Fluid Flow, Heat Transfer, and Deformation in Fractured Porous Rock, *International Journal of Rock Mechanics and Mining Sciences*, 39, 429–442.
- van Genuchten, MT, 1980. A closed-form equation for predicting the hydraulic conductivity of unsaturated soils. *Soil Sci Soc Am J.* 44, 892-898.
- Wolters R., K.-H. Lux, and U. Düsterloh, 2012. Evaluation of Rock Salt Barriers with Respect to Tightness: Influence of Thermomechanical Damage, Fluid Infiltration and Sealing/Healing. *SaltMech7* (p. 10). Paris: Balkema, Rotterdam.